Chemical Geology 607 (2022) 121015

Contents lists available at ScienceDirect

Chemical Geology

journal homepage: www.elsevier.com/locate/chemgeo

A detailed and comprehensive TEM, EPMA and Raman characterization of high-metamorphic grade monazites and their U-Th-Pb systematics (the Góry Sowie Block, SW Poland)

Bartosz Budzyń [a,*], Richard Wirth [b], Jiří Sláma [c], Gabriela A. Kozub-Budzyń [d], Grzegorz Rzepa [d], Anja Schreiber [b]

[a] Institute of Geological Sciences, Polish Academy of Sciences, Research Centre in Kraków, Senacka 1, PL 31002, Kraków, Poland
[b] GeoForschungsZentrum Potsdam (GFZ), Section 3.5 Interface Geochemistry, Telegrafenberg, Potsdam 14473, Germany
[c] The Czech Academy of Sciences, Institute of Geology, Rozvojová 269, Prague 6 16500, Czech Republic
[d] AGH University of Science and Technology, Faculty of Geology, Geophysics and Environmental Protection, al. A. Mickiewicza 30, PL 30059, Kraków, Poland

ARTICLE INFO

Editor: Balz Kamber

Keywords:
Monazite stability
Mineral-fluid reactions
Dissolution-reprecipitation processes
Radiation damage
Common Pb contamination
LA-ICPMS U-Th-Pb isotopic dating

ABSTRACT

Eleven monazite grains, two from a migmatitic gneiss and nine from two felsic granulites from the Góry Sowie Block (SW Poland) were studied with transmission electron microscopy (TEM), electron probe microanalysis (EPMA), Raman microspectroscopy and laser ablation inductively coupled plasma mass spectrometry (LA-ICPMS) U-Th-Pb analysis in order to assess processes affecting U-Th-Pb age record. Two monazite grains from the migmatitic gneiss are patchy zoned in BSE imaging and overgrown by allanite, whereas Raman results indicate moderate radiation damage. Monazite in the corresponding TEM foils shows twins and nanoinclusions of fluorapatite, thorianite, goethite, titanite, chlorite and $CaSO_4$. Furthermore, monazite is partially replaced by secondary monazite, forming ca. 100 nm-thick layers, and calcite along grain boundaries. The submicron alterations had little or no effect on the Pb/U and Pb/Th dates, when compared to earlier age constraints on the metamorphism in the studied region. In contrast, monazite from both granulites is homogeneous in eight investigated TEM foils, contains no solid or fluid nanoinclusions or any signs of fluid-induced alterations, with only one exception of a ca. 140 nm-thick crack filled with monazite. The $^{206}Pb/^{238}U$ and marginally older $^{208}Pb/^{232}Th$ mean dates pulled for all data show good coherence. However, the $^{207}Pb/^{235}U$ isotopic record is disturbed due the presence of common Pb within the entire monazite grain in one granulite and in the cores of two monazite grains in the second granulite, where the U—Pb data of the rims are not compromised and concordant. Due to lack of TEM evidence for fluid-mediated alterations, the age discordance has to be related to addition of common Pb in the monazite lattice or in the micro-cracks. To summarize, the $^{208}Pb/^{232}Th$ data reveal the most accurate ages, which are consistent with previous geochronological studies in the region. Therefore, the Pb/Th chronometer, which is less compromised by age disturbance compared to Pb/U ages, is recommended for monazite geochronology. Application of the submicron scale investigations using TEM is recommended to evaluate potential presence of the submicron inclusions of Pb-bearing phases or compositional alterations of monazite that can remain unnoticed by using standard microanalytical instruments.

1. Introduction

Monazite-(Ce) ((LREE, Th, U)PO_4, henceforth monazite) is one of the main carriers of rare earth elements (REE) in the Earth's crust and a common accessory phase in igneous and metamorphic rocks. Monazite is among most frequently used geochronometers for dating metamorphic processes with LA-ICPMS or SIMS U-Th-Pb measurements (Kylander-Clark, 2017; Schmitt and Vazquez, 2017) or U-Th-total Pb electron probe microanalysis (Williams et al., 2017). Despite high contents of Th and U, monazite shows only low- to moderate degree of metamictization due to high-radiation resistance related to a low damage-annealing temperature (Seydoux-Guillaume et al., 2018b; Nasdala et al., 2020). Monazite is characterized by a very slow solid state diffusion of U, Th and Pb up to high temperatures, whereas interactions

* Corresponding author.
E-mail address: ndbudzyn@cyf-kr.edu.pl (B. Budzyń).

https://doi.org/10.1016/j.chemgeo.2022.121015
Received 21 March 2022; Received in revised form 26 May 2022; Accepted 8 July 2022
Available online 12 July 2022

with fluids can disturb the U-Th-Pb age record (Cherniak et al., 2004; Gardés et al., 2006). Fluid-induced coupled dissolution-reprecipitation processes can result in partial to complete removal of Pb and resetting the original age even at low temperature conditions of 250–550 °C (Williams et al., 2011; Budzyń et al., 2015, 2021b; Grand'Homme et al., 2016, 2018). A recent experimental study revealed that U-Th-Pb dates can be disturbed via fluid-mediated alterations of monazite at 750 °C, which occur extensively at the submicron scale with the formation of high density of fluid and cheralite nanoinclusions that remain unnoticed using standard SEM or EPMA imaging (Budzyń et al., 2021b).

In-situ isotope U-Th-Pb monazite geochronology is increasingly used due to improvement and increasing availability of LA-ICPMS and SIMS techniques, as well as availability of the reference materials (e.g., Gonçalves et al., 2016, 2017; Budzyń et al., 2021a). Common high contents of Th and U at the level of at least 1000 ppm allow us using analytical spot size <10 μm to measure growth or altered domains of monazite and constrain the age of the separate geological processes, which has been earlier mostly obtained by EPMA with spot size <1 μm (Williams et al., 2017). At least several factors may affect Pb/U and Pb/Th isotope systematics in monazite and result in age disturbance. The $^{207}Pb/^{235}U$ ratio is sensitive to common Pb additions due to low ^{235}U abundance, and consequently low content of radiogenic ^{207}Pb in monazite, compared to ^{208}Pb and ^{206}Pb isotopes. The $^{206}Pb/^{238}U$ ratio can be affected by initial ^{206}Pb excess related to ^{230}Th disequilibrium due to very high contents of Th in monazite (Schoene, 2014). Transmission electron microscopy (TEM) has particular importance in case of the presence of nanoinclusions, such as Pb-rich nanoinclusions or nanodomains accumulating unsupported Pb, that may interfere with the U-Th-Pb isotopic record of monazite (Seydoux-Guillaume et al., 2012, 2018a). Submicron investigations can provide answers for our better understanding of the mechanisms inducing the discordant ages or concordant dates spread along the concordia curve, however, processes affecting monazite in the nanoscale are still not sufficiently well understood.

This study focuses on the submicron processes that may affect monazite U-Th-Pb isotope characteristics in high-grade metamorphic rocks. For this purpose, we selected monazite from a well characterized region to control accuracy of Pb/U and Pb/Th age constraints and, more specifically, previously investigated samples are studied to shed more light on the submicron features of monazite and their effect on U-Th-Pb isotope characteristics. Migmatitic gneisses and granulites of the Góry Sowie Block (NE Bohemian Massif, SW Poland) have been studied for decades with respect to their P-T-t records (Kryza, 1981; Żelaźniewicz, 1990; O'Brien et al., 1997; Bröcker et al., 1998; Marheine et al., 2002; Gordon et al., 2005; Schneider et al., 2006; Kryza and Fanning, 2007; Budzyń et al., 2018; Jastrzębski et al., 2021), making this area an excellent natural laboratory for investigating monazite behavior during prolonged metamorphic episodes. Here, we studied monazite in a migmatitic gneiss and two granulites to address, among others, the following: (i) if monazite overgrown by allanite in migmatitic gneiss is also affected by the internal submicron alterations that may compromise U-Th-Pb ages, and (ii) if there is evidence of submicron processes that resulted in discordance of the U-Th-Pb monazite ages in granulites that underwent ultra-high temperature metamorphic overprint during decompression. TEM investigations allowed us to constrain submicron evidence of the processes, which potentially may affect a Th-U-Pb age record (or lack of such), whereas the degree of radiation damage was estimated with Raman microspectroscopy. Extensive LA-ICPMS U-Th-Pb analyses allowed us to investigate distribution and preservation of isotopic records within individual monazite grains. To summarize, this work focuses selection of advanced analytical techniques on the small number of grains to expand our understanding of monazite behavior during high-grade metamorphic processes and their implications into U-Th-Pb geochronology.

2. Samples and methods

2.1. Geological background and sample description

The Góry Sowie Block, located in the central part of the central Sudetes (NE Bohemian Massif, SW Poland), consists of migmatitic para- and orthogneisses, amphibolites, and minor granulites, pegmatites, garnet metaperidotites and calc-silicate rocks (Kryza, 1981; Żelaźniewicz, 1990). The unit experienced several (up to five) tectonic and metamorphic events (Żelaźniewicz, 1990; see Jastrzębski et al., 2021 for a review of previous studies), which can be briefly summarized to:

- high pressure–high temperature (HP-HT) granulite facies metamorphic event ca. 400–395 Ma (O'Brien et al., 1997; Gordon et al., 2005; Kryza and Fanning, 2007; Tabaud et al., 2020),
- amphibolite facies migmatization ca. 385–370 Ma (Gordon et al., 2005; Kryza and Fanning, 2007; Budzyń et al., 2018; Tabaud et al., 2020; Jastrzębski et al., 2021),
- rapid cooling ca. 370–360 Ma (Bröcker et al., 1998; Marheine et al., 2002; Schneider et al., 2006).

The current work presents a comprehensive study of eleven monazite grains from the migmatitic gneiss and two felsic granulites, which were recently studied in terms of thermodynamic modeling and monazite geochronology (Jastrzębski et al., 2021). The migmatitic gneiss SUD1 from Piława Górna (50°42′15.7″N 16°44′11.5″E) contains quartz, plagioclase, K-feldspar and biotite, with rare muscovite and accessory garnet, monazite, allanite, apatite, zircon, ilmenite and titanite. Thermodynamic modeling constrained P-T conditions of 5–6 kbar/680–690 °C, followed by 3.5–4.5 kbar/ca. 700 °C; monazite yielded a concordia age of 378.1 ± 5.5 Ma (95% conf., MSWD = 0.12; Jastrzębski et al., 2021). Two monazite grains, selected for the current study, show patchy to sector zoning and are partially replaced by allanite (Fig. 1a, b); previous U—Pb dates have −2.5 to −0.5% disc. (discordance). One of the monazite grains (Mnz2) contains inclusions of ilmenite.

The felsic granulite GS290B from Bystrzyca Górna (50°46′37″N 16°27′07″E) is composed of quartz, plagioclase, K-feldspar, garnet, kyanite, biotite and rutile. Monazite yielded a concordia age of 385.9 ± 8.0 Ma (95% conf., MSWD = 0.04), whereas P-T conditions in a similar granulite from this locality were constrained to 17–18 kbar/740–750 °C followed by decompression and heating to 11–12 kbar/830–840 °C (Jastrzębski et al., 2021). For this work, two monazite grains reflecting growth zoning (Fig. 1c, d) were selected, as representative for less (−2.5 and 0.5% disc.; Mnz1) and more discordant (9.4 and 9.7% disc.; Mnz2) U—Pb dates in a previous investigation.

The felsic granulite SUD43 from the exposure near the Fregata Hostel (the Bystrzyckie lake near Zagórze Śląskie, 50°45′08.1″N 16°26′07.4″E) is composed of quartz, plagioclase, K-feldspar, garnet, kyanite, biotite and rutile. The SUD43 sample was chosen due to a high abundance of monazite grains, which demonstrate distinct core-rim relations and have record of concordant to discordant dates due to incorporation of common Pb (Jastrzębski et al., 2021). Monazite yielded the lower intercept age 369.6 ± 1.6 Ma (2σ, MSWD = 0.36), which is consistent with a U—Pb concordia age of 370.0 ± 5.1 Ma (2σ, MSWD = 0.15) pulled by most concordant data (Jastrzębski et al., 2021). Two monazite grains (Mnz1 and Mnz2) that previously yielded dates with −2.1 to 15.1% disc. have been selected for TEM and Raman microspectroscopy. These two grains and additional five monazite grains, previously not investigated, have been chosen for extensive LA-ICPMS U-Th-Pb measurements (Fig. 1e–k).

2.2. Analytical methods

Backscattered electron (BSE) imaging and compositional analyses of monazite in thin sections (SUD1, GS290B) and polished 1″ grain mount

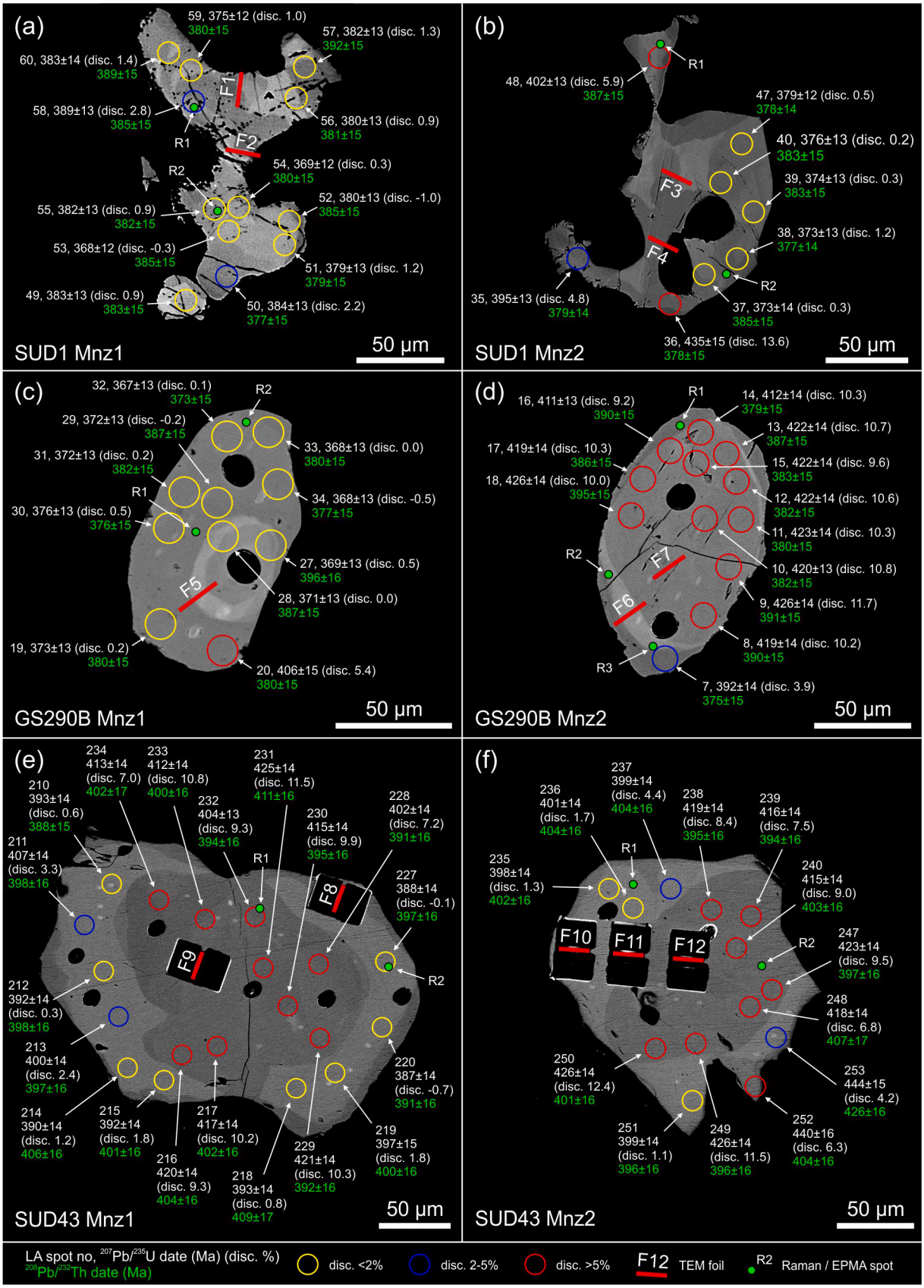

Fig. 1. BSE images of the investigated monazite grains from the migmatitic gneiss (a, b) and two felsic granulites (c–k). Discrepancy between $^{207}Pb/^{235}U$ and $^{208}Pb/^{208}Th$ dates (i.e., older $^{207}Pb/^{235}U$ dates) is related to the presence of common Pb mostly affecting $^{207}Pb/^{235}U$ ratio due to lower concentrations of ^{235}U.

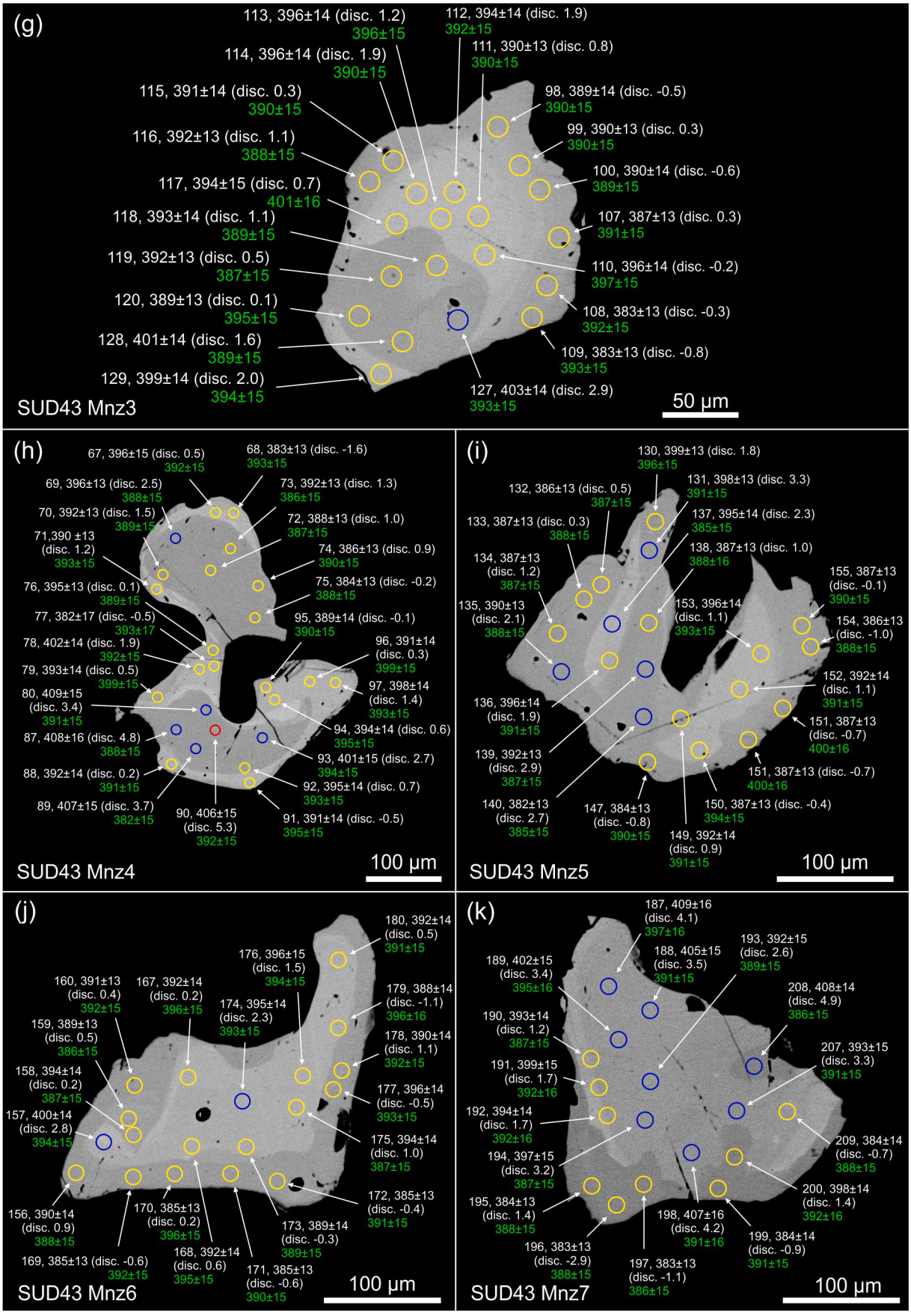

Fig. 1. (*continued*).

(SUD43) were performed using a JEOL SuperProbe JXA-8230 electron microprobe at the Laboratory of Critical Elements AGH–KGHM at the AGH University of Science and Technology (Kraków, Poland). Analytical conditions included an accelerating voltage of 15 kV, a probe current of 100 nA and a beam size of 3 μm. See Supplementary Table S1 for counting times, standards used, spectral lines and WDS crystals. Data were corrected using an in-house ZAF procedure.

Sample preparation for TEM was performed by focused ion beam (FIB) milling at the German Research Centre for Geosciences (GFZ Potsdam) using a HELIOS G4 UC FIB/SEM system. An area of 20 × 2 μm on each sample was selected. The final size of the FIB-foils cut directly from the grains in the carbon-coated thin sections was approximately 20 × 10 × 0.1 μm (see Wirth, 2004, 2009 for details of the sample preparation). Transmission electron microscopy observations were performed using a FEI Tecnai G2 F20 X-Twin TEM with a Schottky field emitter as an electron source. The TEM was equipped with a Fishione high-angle annular dark field detector, an EDAX X-Ray analyzer and a Gatan electron energy-loss spectrometer. The TEM procedures applied follow those used in our recent study (Budzyń et al., 2021b).

U-Th-Pb measurements in monazite were performed using a Thermo Scientific Element 2 sector field ICP-MS coupled to a 193 nm ArF excimer laser (Teledyne Cetac Analyte Excite laser) at the Institute of Geology of the Czech Academy of Sciences. The procedure follows closely that described in Budzyń et al. (2021a). The laser was fired at a repetition rate of 5 Hz with a fluence of 1.7 J/cm^2 and a spot size of 13 μm. Detailed analytical conditions are presented in Supplementary Table S2. The U-Th-Pb data are presented as concordia and mean plots generated with ISOPLOT v. 4.16 (Ludwig, 2012).

Raman microspectroscopy measurements of monazite were conducted using a Thermo Scientific DXR Raman Microscope at the Faculty of Geology, Geophysics and Environmental Protection, AGH University of Science and Technology (Kraków, Poland). The analyses were performed prior to EPMA and LA-ICPMS measurements. The spectra were collected at room temperature using a green, 532 nm diode laser with a power of 10 mW focused through an Olympus 100× objective resulting is spot size of ca. 0.7 μm. Acquisitions were obtained with a 900 grooves/mm grating and a CCD detector. An exposure time of 3 s and 100 data accumulations were used. The spectra were fitted after background correction assuming Gaussian-Lorentzian band shape (Ruschel et al., 2012). The measured FWHMs (full width at half maximum) values of monazite $\nu_1(PO_4)$ stretching band at ca. 971–973 cm^{-1} were corrected for instrumental broadening (Nasdala et al., 2001).

3. Results

3.1. TEM, EPMA and Raman microspectroscopy

Two investigated monazite grains from the migmatitic gneiss contain 4.14–4.44 wt% ThO_2 and 0.22–0.44 wt% UO_2 (Supplementary Table S3). The FWHM (full width at half maximum) values 11.67–12.69 cm^{-1} of the Raman $\nu_1(PO_4)$ stretching band, which are approximately twice higher than FWHM values 5.99–6.23 cm^{-1} indicate moderate radiation damage calculated on the basis of Th, U, Ca and Pb contents (after Ruschel et al., 2012) (Fig. 2; Supplementary Table S4). Monazite Mnz1 has irregular xenomorphic shape with no core-rim textural relation. Two TEM foils represent transitions between patchy zones (Fig. 1a) and, to lesser extent, grain boundary partially overgrown by allanite. Foil F1 represents homogeneous monazite with no inclusions, except one fluid inclusion with little Fe enrichment (Fig. 3a, b). In contrary, foil F2 includes monazite and secondary allanite, overgrowing monazite, which are partially dissolved (Fig. 3c, d). Monazite contains submicron inclusions of fluorapatite, thorianite and goethite (Fig. 3e–j), and fluid inclusions. Fluorapatite is well crystalline and forms inclusions sizing from ca. 150 × 600 nm to ca. 1 μm (Fig. 3e–g, j). Thorianite inclusions occur in low abundance and their size is below 0.5 μm (Fig. 3g).

Two TEM foils were cut from monazite Mnz2, also from the migmatitic gneiss, across two sector zones (F3) and across a phase boundary with an ilmenite inclusion (F4; Fig. 1b). Foil F3 presents polycrystalline monazite forming twins with partially open grain boundaries, along which ThO_2 nanoparticles crystallized (Fig. 4a–d). Monazite displays high crystallinity with just minor mottled diffraction contrast in HREM imaging (Fig. 4f), and undistorted, sharp diffraction patterns (Fig. 4j). Inclusions of other phases are rare in the foil. These include nanoinclusions of titanite, chlorite and $CaSO_4$ (Fig. 4e–i).

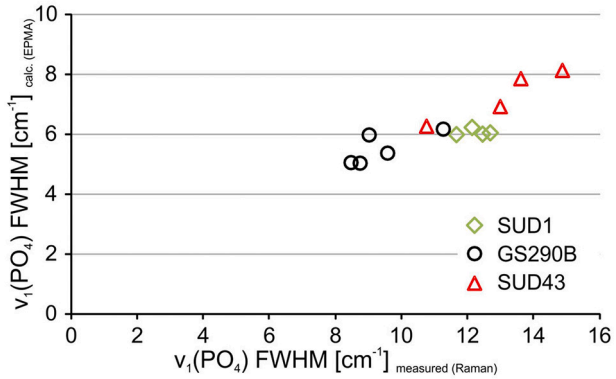

Fig. 2. Diagram presenting the FWHM (full width at half maximum) of measured $\nu_1(PO_4)$ symmetric stretching band (Raman) vs. calculated values using compositional data (EPMA) that represent "chemical broadening" of the $\nu_1(PO_4)$ band (Ruschel et al., 2012). High measured FWHM values indicate moderate degree of metamictization due to radiation damage.

The second foil of Mnz2 (F4) displays twins and a partially open grain boundary between monazite and an inclusion of ilmenite (Fig. 5a–c). Monazite is homogeneous and contains no inclusions except those along grain boundaries, where calcite and probably goethite formed (Fig. 5d, e, h, j, l). Here, monazite is partially altered with Ca-enrichment and Th-depletion (Fig. 5a–g). Altered monazite shows mottled diffraction contrast in HREM imaging and slightly diffuse diffraction patterns thus indicating irradiation damage (Fig. 5g, i, k).

Two monazite grains from the felsic granulite GS290B show growth zoning, and contain 1.71–4.03 wt% ThO_2 and 0.38–1.17 wt% UO_2 (Supplementary Table S3). FWHM values 8.47–11.27 cm^{-1} of the Raman $\nu_1(PO_4)$ stretching band indicate low to moderate radiation damage (Fig. 2; Supplementary Table S4). Foils F5 and F6 cut across three compositional domains from core to rim of grains Mnz1 and Mnz2, respectively, display homogeneous monazite with no inclusions and no grain boundaries (Fig. 6a–d). The same features demonstrate foil F7 from the Mnz2 core, except an approximately 120 nm-thick crack filled with monazite (Fig. 6e-g).

Monazite from felsic granulite SUD43 shows distinct core-rim relations (Fig. 1e–k) with ThO_2 and UO_2 varying from 4.39 to 10.08 wt% and 0.18–0.98 wt%, respectively (Supplementary Table S3). FWHM values of the Raman $\nu_1(PO_4)$ stretching band 10.76–14.87 cm^{-1} are significantly higher than FWHM values 6.27–8.18 cm^{-1} thus indicating moderate radiation damage calculated on the basis of monazite composition (Fig. 2; Supplementary Table S4). Five foils (F9–F12) from two grains demonstrate homogeneous monazite in cores and rims with no inclusions or grain boundaries (Fig. 6h–l).

3.2. LA-ICPMS U-Th-Pb analysis

LA-ICPMS U-Th-Pb measurements were performed in 11 monazite grains, 8–25 analyzes per grain depending on the grain size. Analytical strategy of the measurements covered all distinguished domains to investigate potential variations of dates and their discordance values. In this work, a 2% discordance (disc.) criterion is used to distinguish between the most concordant and other data, in contrast to commonly used 5 or 10% disc. criterion for U—Pb ages <1 Ga. This allowed us to

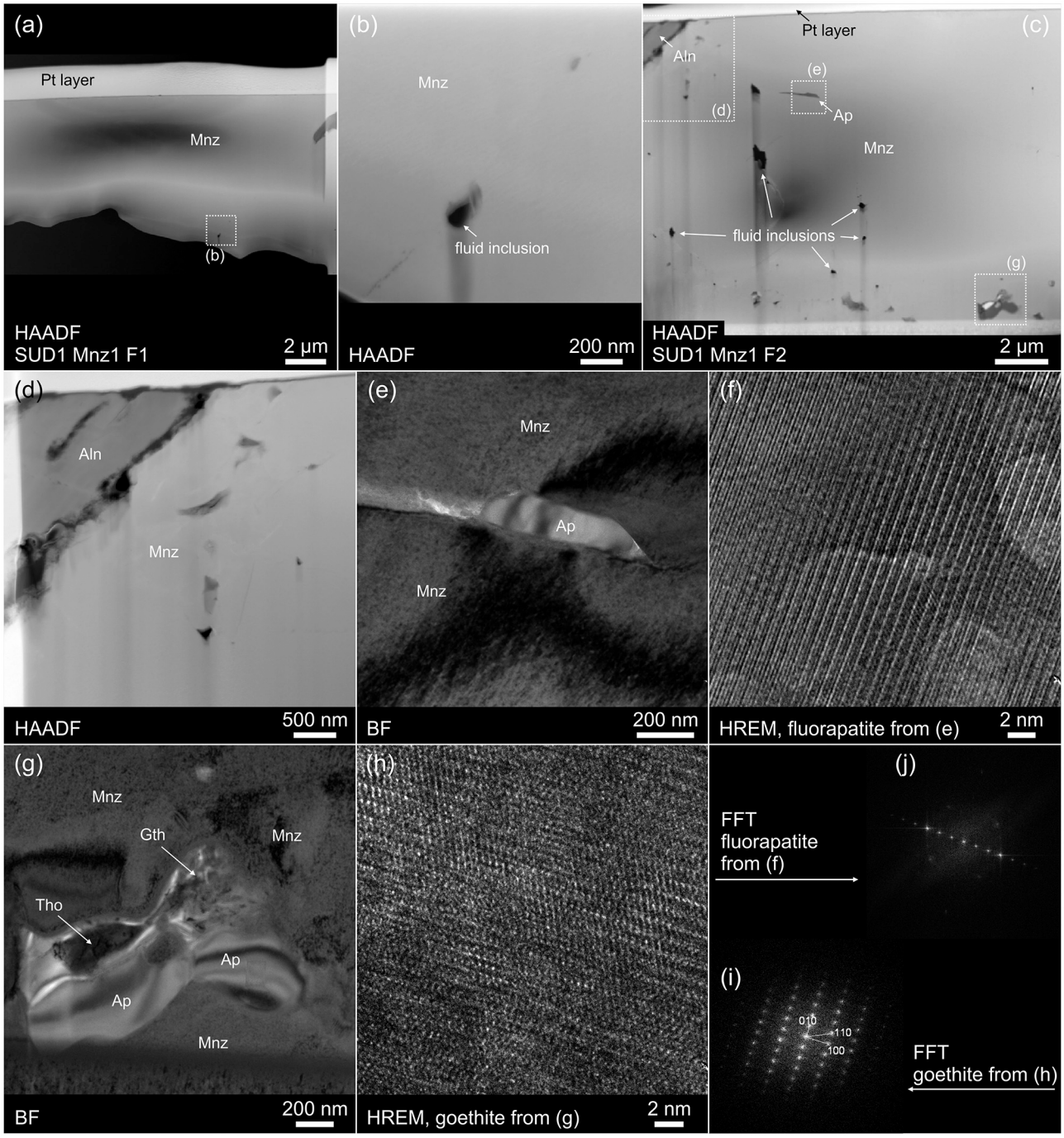

Fig. 3. TEM images demonstrating homogeneous monazite (from the migmatitic gneiss SUD1) in foil F1 (a,b) and nanoinclusions of foreign phases and fluid in monazite in foil F2 (c–j). See text for more details. (a–d) are HAADF images; (e, g) are bright-field images; (f, h) are high resolution lattice fringe images; (i, j) are diffraction patterns. Aln – allanite, Ap – fluorapatite, Gth – goethite, Mnz – monazite, Tho – thorianite.

push the limits in using most concordant dates in the discussion. Concordia plots present data highlighted for <2, 2–5 and > 10% disc. criterions (Fig. 7), whereas mean dates are presented for all data and data <2% disc. (Figs. 8–9). The complete U-Th-Pb dataset is available from Supplementary Table S5.

Two monazite grains from the migmatitic gneiss yielded U-Th-Pb data mostly from −1.0 to 1.4% disc. (n = 15), whereas five analyses yielded dates with 2.2–13.6% disc. and minor addition of common Pb (Fig. 7a–b). In general, analyses in both grains yielded a similar set of uniform dates for each isotopic ratio. Only two $^{207}Pb/^{235}U$ discordant dates 402 ± 13 and 435 ± 15 Ma are older than most of the $^{207}Pb/^{235}U$ data ranging from 368 ± 12 to 395 ± 13 Ma (Fig. 8a). All calculated mean dates are within 2σ error, and corresponding means pulled for all data and data <2% disc. for each isotopic ratio are within <2 Ma difference (Fig. 8d–f). The $^{207}Pb/^{235}U$ and $^{206}Pb/^{238}U$ mean dates (<2% disc.) 376.9 ± 6.9 Ma (MSWD = 0.14) and 374.8 ± 8.3 Ma (MSWD = 0.076), respectively, are only slightly younger than $^{208}Pb/^{232}Th$ mean date 383 ± 11 Ma (MSWD = 0.039; Fig. 8d–f), and all are in agreement with the lower intercept age 375.0 ± 4.2 Ma (MSWD = 0.25) pulled for all data (Fig. 7a). The important result is that corresponding $^{206}Pb/^{238}U$ and $^{208}Pb/^{232}Th$ means pulled for all data and data <2% disc. are nearly the same (Fig. 8b, c, e, f).

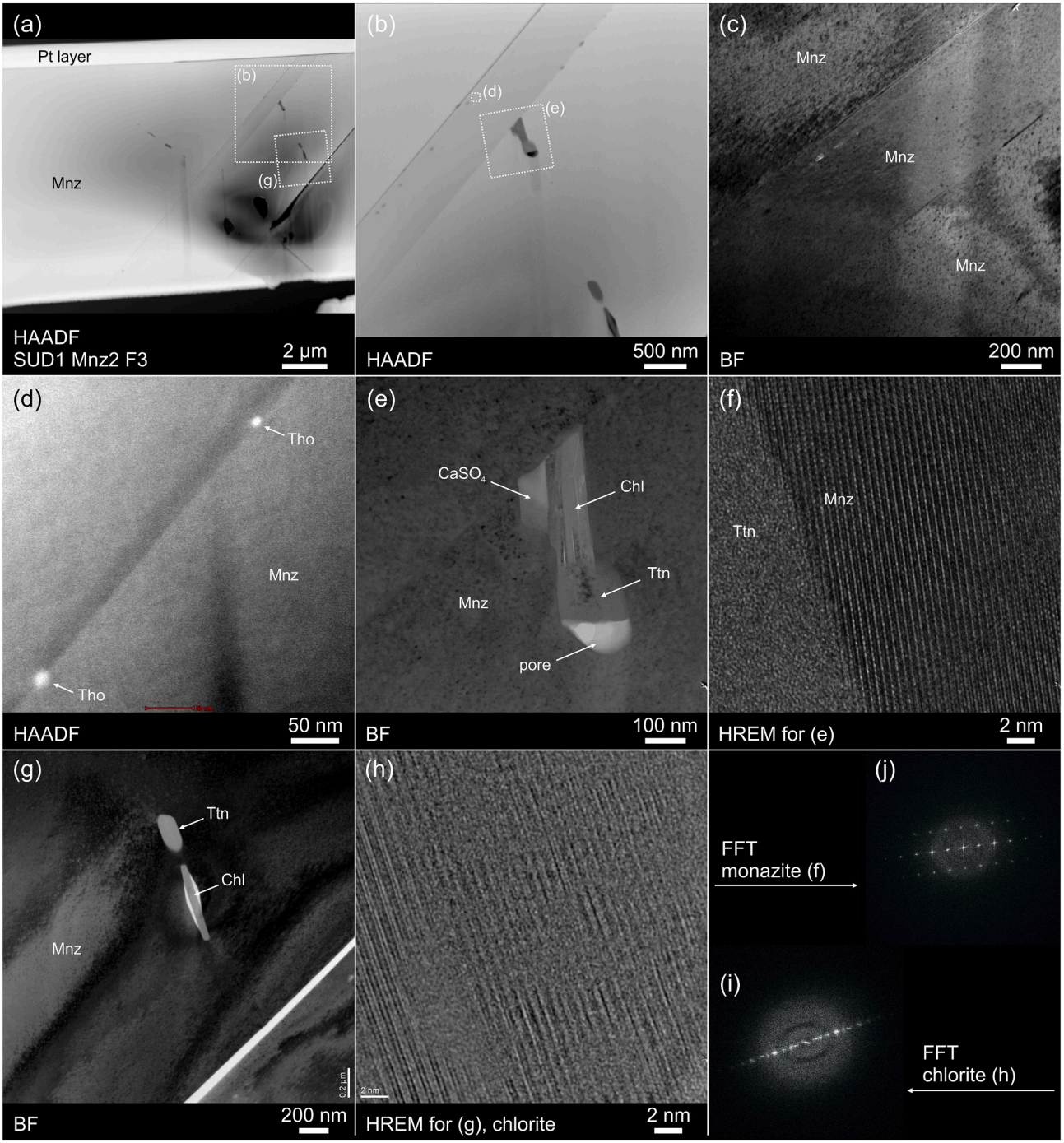

Fig. 4. TEM images demonstrating homogeneous monazite (from the migmatitic gneiss SUD1) in foil F3. Monazite displays twins with nanoinclusions of thorianite (Tho), $CaSO_4$, chlorite (Chl) and titanite (Ttn) formed along the closed grain boundaries. See text for more details. (a, b, d) are HAADF images; (c, e, g) are bright-field images; (f, h) are high-resolution lattice fringe images. (i, j) are diffraction patterns.

Monazite U-Th-Pb data from the granulite GS290B show a discrepancy between two investigated grains. The first monazite Mnz1 yielded 9 nearly uniform $^{207}Pb/^{235}U$ dates from 367 ± 13 to 376 ± 13 Ma with discordance from −0.5 to 0.5%, and one older $^{207}Pb/^{235}U$ date 406 ± 15 Ma (5.4% disc.). Here, all $^{206}Pb/^{238}U$ and $^{208}Pb/^{232}Th$ dates are in the similar ranges shifted towards older dates from 367 ± 15 to 384 ± 15 Ma and from 373 ± 15 to 396 ± 16 Ma, respectively. Monazite Mnz2 provided more discordant data with $^{207}Pb/^{235}U$ dates ranging from 392 ± 14 to 426 ± 14 Ma (3.9–11.7% disc.). The younger ranges of $^{206}Pb/^{238}U$ and $^{208}Pb/^{232}Th$ dates are from 369 ± 14 to 383 ± 15 Ma and from 375 ± 15 to 395 ± 15 Ma, respectively, which is similar to data from Mnz1. There are no discrepancies between U-Th-Pb data from cores and rims. The $^{207}Pb/^{235}U$ and $^{206}Pb/^{238}U$ means calculated using dates <2% disc. are 370.6 ± 9.0 Ma (MSWD = 0.047) and 370 ± 11 Ma (MSWD = 0.025), which is approximately the same as a lower intercept age 371.0 ± 5.5 Ma (MSWD = 0.22), and overlap in the uncertainty range with slightly older $^{208}Pb/^{232}Th$ mean 382 ± 14 Ma (MSWD = 0.109; Figs. 7c, 8j–l). The important observation is that $^{208}Pb/^{232}Th$ means 383.5 ± 8.8 Ma (MSWD = 0.09) and 382 ± 14 Ma (MSWD = 0.109) pulled for all and < 2% disc. data, respectively, are approximately the same (Fig. 8i, j).

Five large monazite grains from the felsic granulite SUD43 were

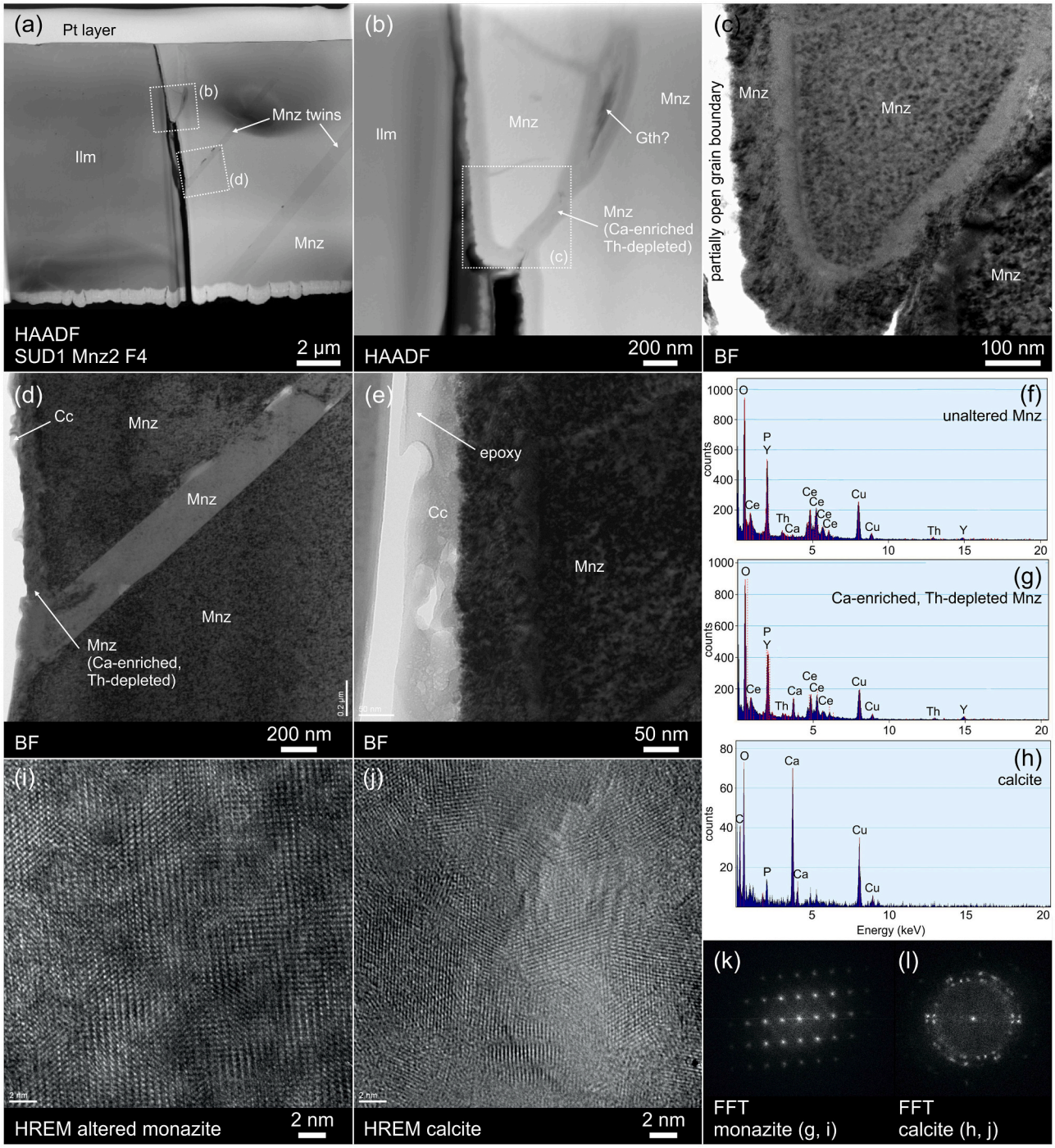

Fig. 5. TEM images demonstrating homogeneous monazite close to the ilmenite (Ilm) inclusion (from the migmatitic gneiss SUD1) in foil F4. Monazite displays a partially open grain boundary along the contact with ilmenite (a–c), and closed grain boundary along the internal crack (b, c) and along twins, which were infiltrated by fluid. Monazite is partially replaced along the grain boundary due to fluid-induced coupled dissolution-reprecipitation, which formed submicron-thick layer of Ca-enriched and Th-depleted secondary monazite, and also calcite (Cc). (a,b) are HAADF images; (c-e) are bright-field images; (i, j) are high-resolution lattice fringe images. (f-h) show results of EDX analyses of monazite and calcite, and (k,l) are corresponding diffraction patterns of monazite and calcite.

measured. Due to distinct textural features and a broader dataset for this sample, the data from cores and rims are discussed separately. Monazite cores yielded $^{207}Pb/^{235}U$ dates from 384 ± 13 to 426 ± 14 Ma (from −1.1 to 12.4% disc.), whereas rims provided a record from 382 ± 13 to 444 ± 15 Ma (from −2.9 to 6.3% disc). The data with discordance above 2% are more abundant in the cores (33/64 analyses) than in the rims (11/69 analyses). Considering all data, $^{207}Pb/^{235}U$ record from 384 ± 14 to 426 ± 14 Ma in the cores is shifted towards older dates compared to $^{206}Pb/^{238}U$ dates ranging from 366 ± 14 to 397 ± 14 Ma and $^{208}Pb/^{232}Th$ dates from 382 ± 15 to 411 ± 16 Ma (Fig. 9a–c). Less discordant data (<2% disc.) are relatively consistent providing $^{207}Pb/^{235}U$, $^{206}Pb/^{238}U$ and $^{208}Pb/^{232}Th$ means 392.2 ± 5.1 Ma (MSWD = 0.077), 389.1 ± 5.9 Ma (MSWD = 0.034) and 391.3 ± 7.6 Ma (MSWD = 0.027), respectively (Fig. 9d–f). In the rims, due to less discordant data compared to the cores, only two analyses provided older $^{207}Pb/^{235}U$ dates 440 ± 16 and 444 ± 15 Ma, which are outside error range of the population. Mean dates calculated for <2% disc. data are within uncertainty range with slightly younger $^{207}Pb/^{235}U$ and $^{206}Pb/^{238}U$ means

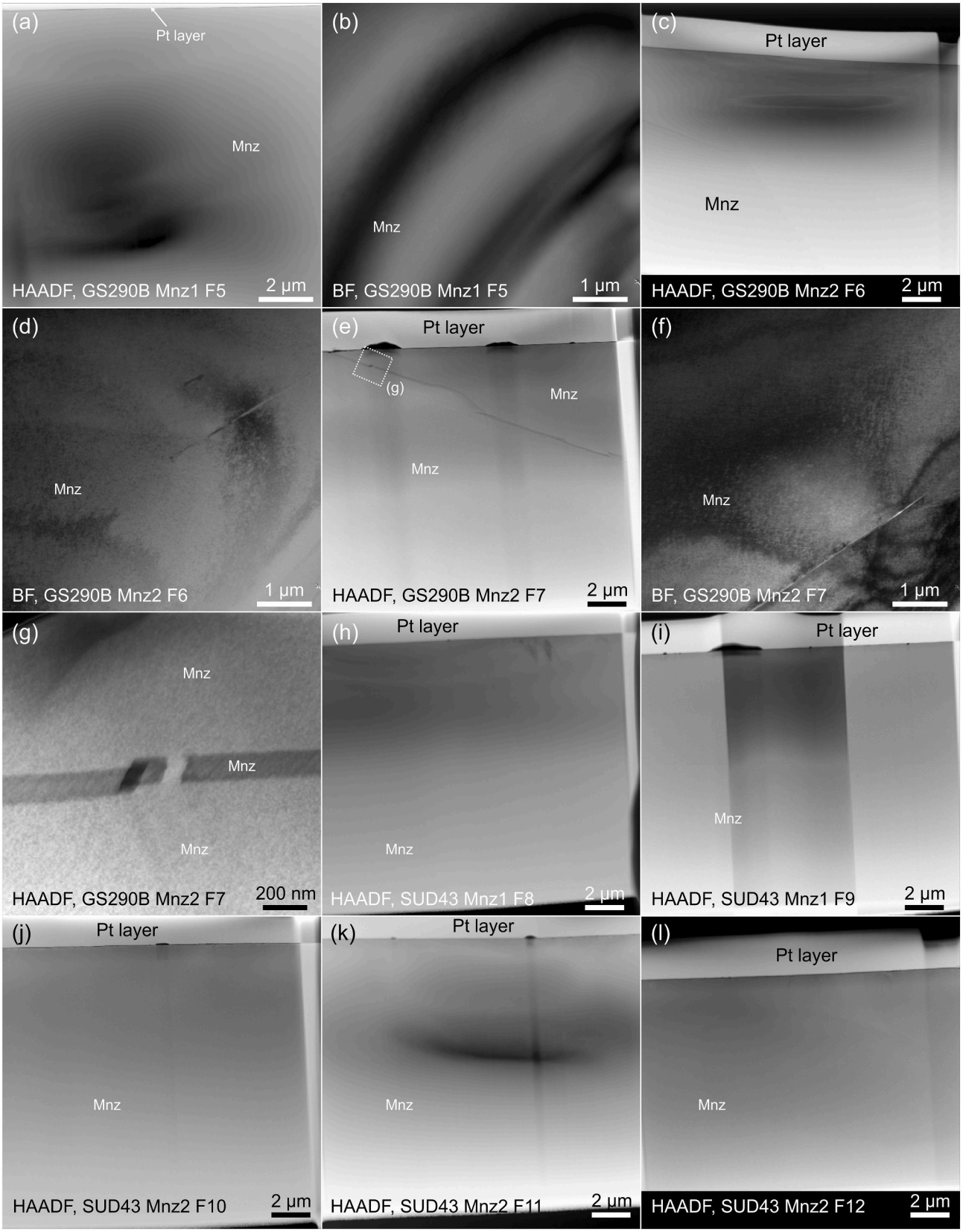

Fig. 6. TEM images of monazite in foils F5–F12 from two felsic granulites GS290B (a–g) and SUD43 (h–l). The monazite is homogeneous and contains no inclusions of fluid or foreign phases. The only exception is the foil F7, which displays crack filled with secondary monazite (e, g). (a, c, e, g–l) are HAADF images. (b, d, f) are TEM bright-field images with diffraction contrast.

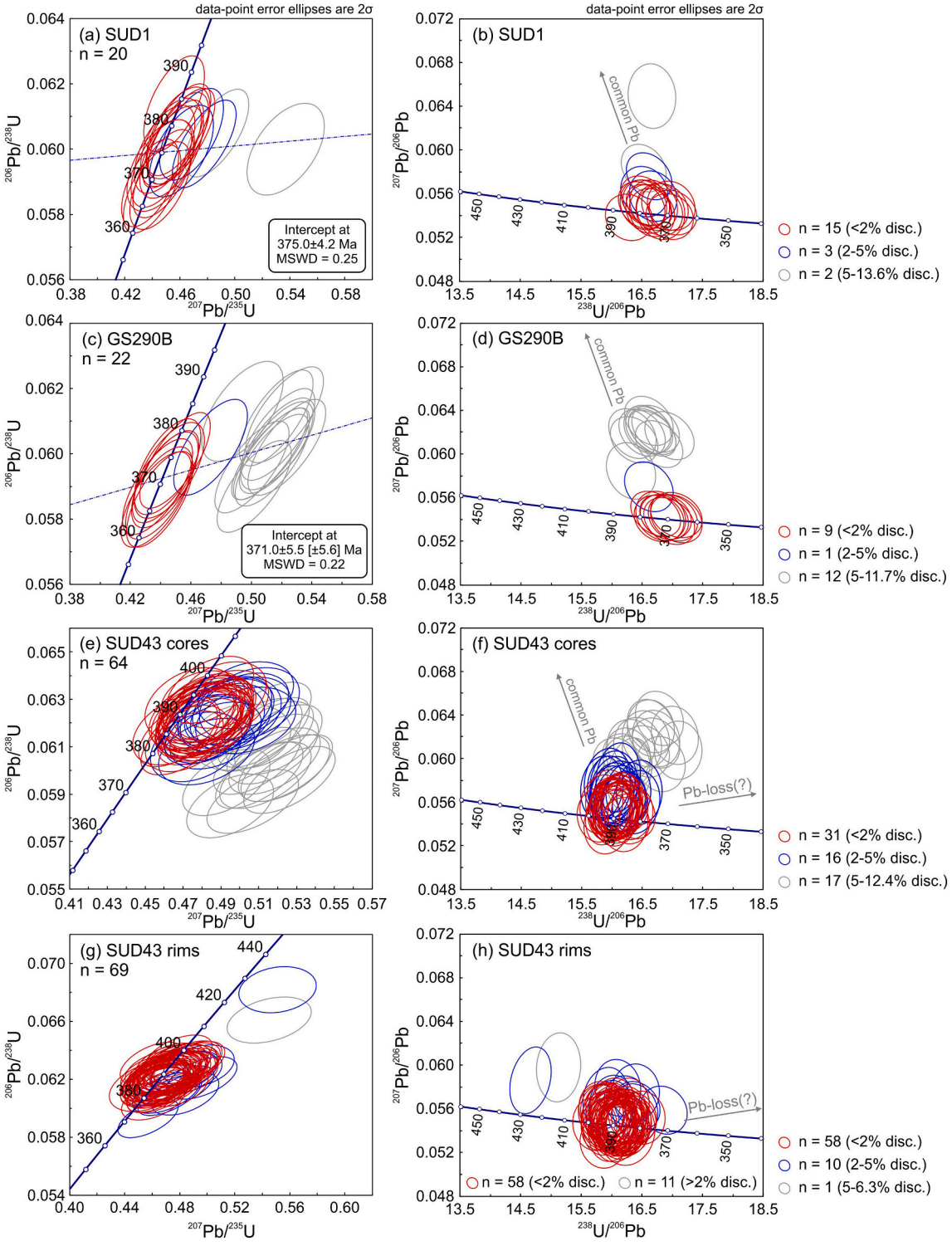

Fig. 7. Wetherill and Terra-Wasserburg concordia diagrams presenting a summary of LA-ICP-MS U—Pb isotopic data. Grey ellipses represent data with >5% disc. partially due to addition of common Pb. Discordance between $^{207}Pb/^{235}U$ and $^{236}Pb/^{238}U$ dates in monazite from granulite SUD43 is due to proportion of common Pb, which is more effective for $^{207}Pb/^{235}U$ ratio, and partially due to limited Pb-loss compromising mostly $^{206}Pb/^{238}U$ ratio. One blue ellipse in (h) possibly represents youngest U—Pb date affected by Pb-loss, however, it is within uncertainty range with concordant dates population. (For interpretation of the references to colour in this figure legend, the reader is referred to the web version of this article.)

389.8 ± 3.7 Ma (MSWD = 0.13) and 388.9 ± 4.4 Ma (MWSD = 0.047), respectively, compared to $^{208}Pb/^{232}Th$ mean 392.5 ± 5.6 Ma (MSWD = 0.054) (Fig. 9j–l).

4. Discussion

The main processes that may affect U-Th-Pb characteristic in monazite include accumulation of common Pb in monazite (Seydoux-Guillaume et al., 2012; Didier et al., 2013; Skrzypek et al., 2017;

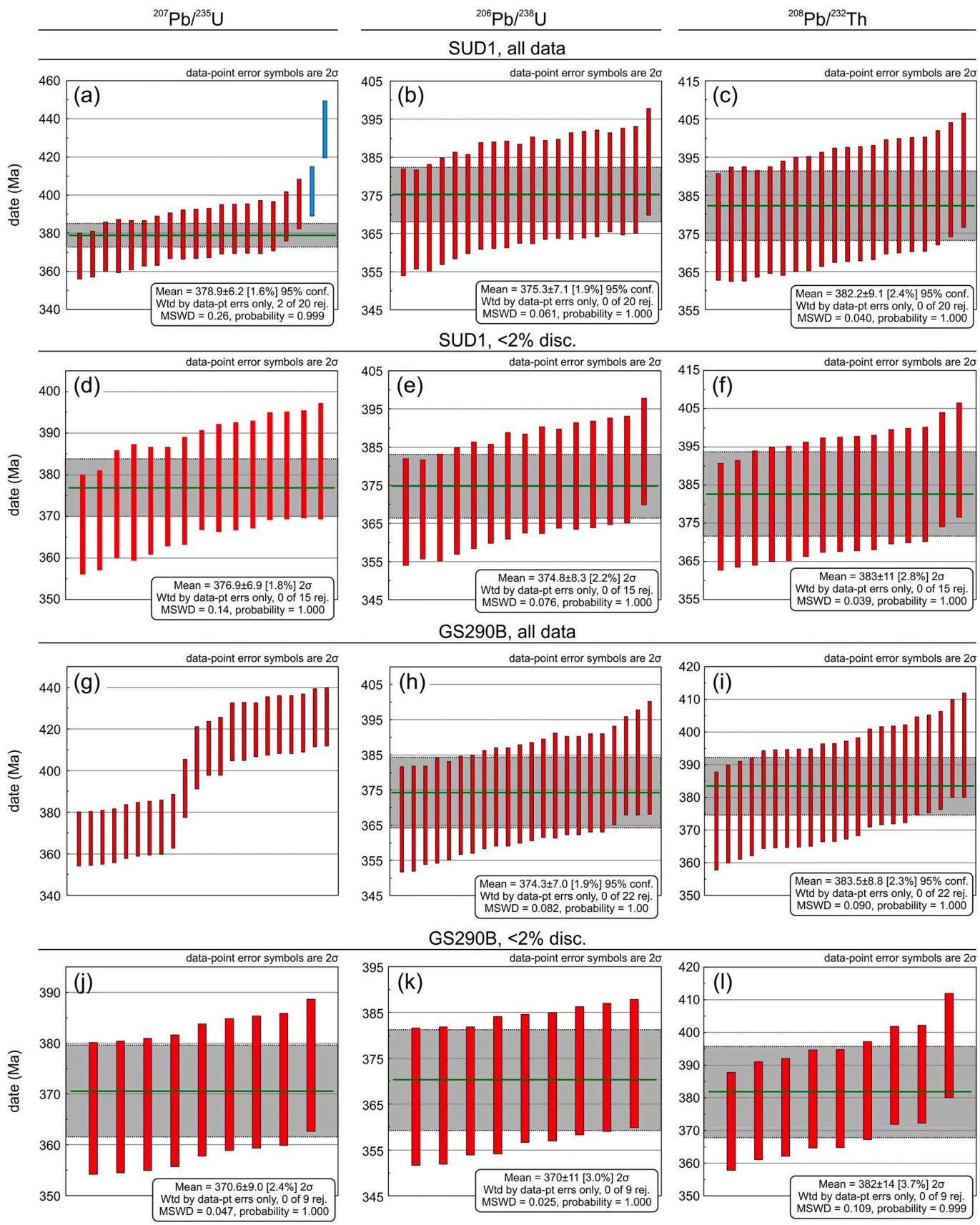

Fig. 8. Results of LA-ICPMS isotopic analyses of monazite from the migmatitic gneiss SUD1 (a–f) and felsic granulite GS290B (g–l) on the diagrams presenting $^{207}Pb/^{235}U$, $^{206}Pb/^{238}U$ and $^{208}Pb/^{232}Th$ mean dates.

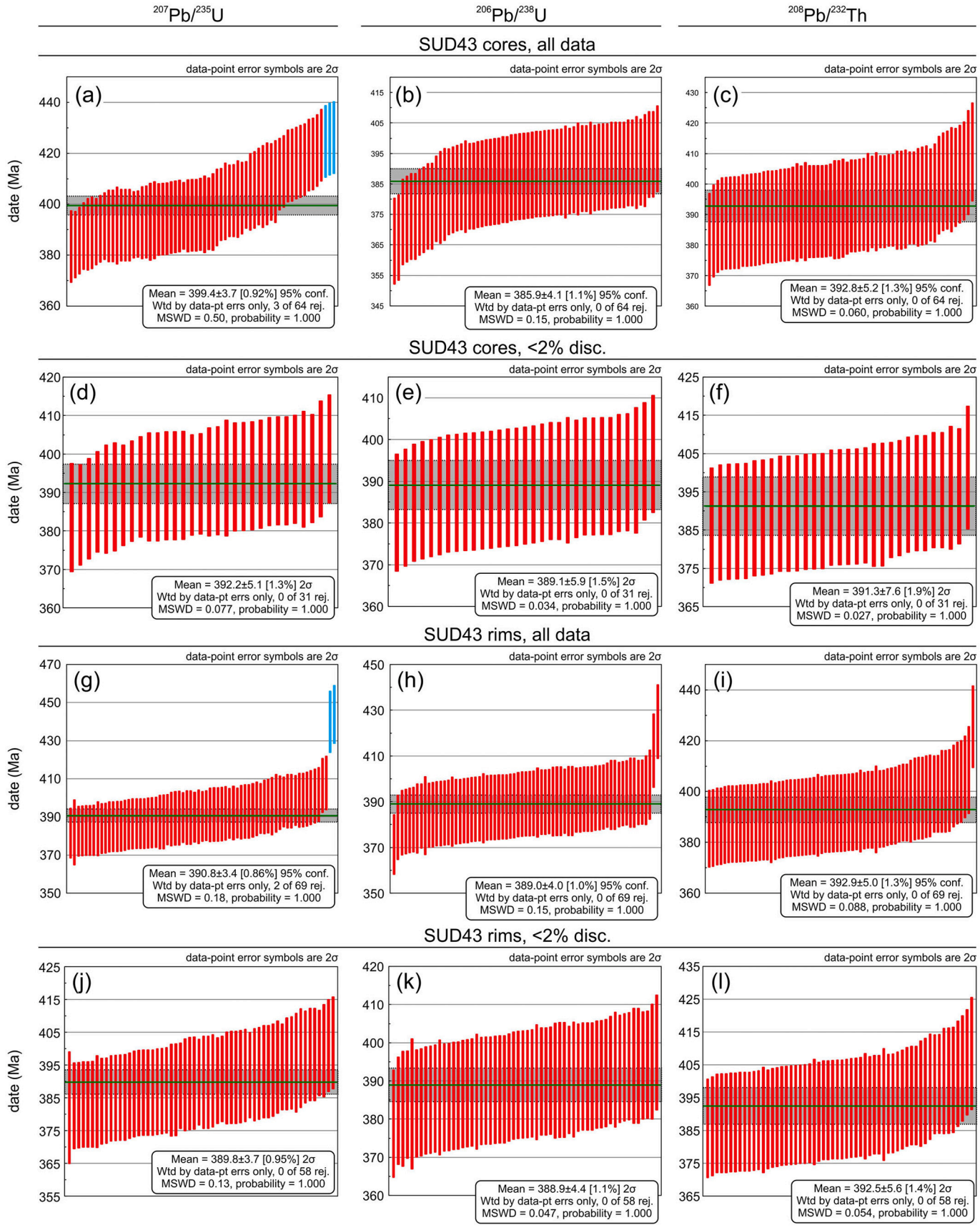

Fig. 9. Results of LA-ICPMS isotopic analyses of monazite from the felsic granulite SUD43 on the diagrams presenting $^{207}Pb/^{235}U$, $^{206}Pb/^{238}U$ and $^{208}Pb/^{232}Th$ mean dates.

Jastrzębski et al., 2020, 2021; Barnes et al., 2021; Budzyń et al., 2021a), low to moderate degree of metamictization related to radiation damage (Seydoux-Guillaume et al., 2018b; Nasdala et al., 2020; Budzyń et al., 2021b), fluid-mediated compositional alteration via coupled dissolution-reprecipitation reactions resulting in removal of Pb in altered monazite domains (Harlov et al., 2011; Williams et al., 2011; Budzyń et al., 2015, 2021b; Grand'Homme et al., 2016, 2018) or the presence of Pb-bearing nanoinclusions (Seydoux-Guillaume et al., 2018a; Turuani et al., 2022). Below we discuss the influence of these on the U-Th-Pb age record and the meaning of the Pb/U and Pb/Th dates in monazite that experienced multiple metamorphic episodes.

4.1. Micro- to submicron-features of monazite

The main features observed in monazite in the migmatitic gneiss SUD1 include (i) the formation of allanite overgrowths on the surface and (ii) internal alterations of monazite observed on the submicron scale. Regarding the first, the relative stabilities of monazite and allanite were intensively studied in the past, and they are controlled primarily by P-T conditions, whole rock composition and the composition of fluids (Broska and Siman, 1998; Finger et al., 1998; Janots et al., 2007, 2008; Spear, 2010; Budzyń et al., 2010, 2011, 2017). The migmatitic gneiss recorded P-T conditions 5–6 kbar/680–690 °C at ca. 380 Ma, followed by 3.5–4.5 kbar/ca. 700 °C, and rapid cooling 370–360 Ma (Jastrzębski et al., 2021). The composition of the gneiss with 1.96 wt% CaO and a bulk CaO/Na_2O ratio of 0.64 (Jastrzębski et al., 2021), allows us to estimate the stability of allanite to temperature conditions below ca. 600 °C (Janots et al., 2008). These estimations together with a small grain size (max. several micrometers) suggest that allanite formed during a rapid cooling event. The retrogressive stage of metamorphism resulted in partial dissolution of the monazite surface, but also of the secondary allanite, and an open grain boundary with submicron-sized cavities between these phases (Fig. 3d). Monazite in migmatitic gneiss SUD1 shows also a partially open grain boundary, up to several hundred nanometers thick, along the contact with ilmenite (Fig. 5a–b). Such open space probably was used for fluid transport that induced monazite alteration via coupled dissolution-reprecipitation process, which resulted in a Ca-enriched and Th-depleted nanometer-scale rim (Fig. 5b–e). Presence of calcite (Fig. 5e, h, j, l) on the monazite surface indicates that the fluid was enriched in CO_2, whereas Ca was supplied either by monazite or fluid, or both. The exceptional case is a closed grain boundary in monazite, which is filled with goethite enclosed in nanometer-scale lamellae of secondary monazite (Fig. 5b). These resulted from fluid penetration along the crack in monazite, which formed due to anisotropic thermoelastic response of the crystal to decompression and cooling at the retrogressive stage of metamorphism (cf., Kruhl et al., 2013; Wirth et al., 2022). The nanometer-scale thick grain boundaries were partially open for fluid also along the lamellas of monazite twins, which resulted in the formation of nanoinclusions of thorianite, titanite, chlorite and $CaSO_4$ (Fig. 4d–i). Monazite supplied Th for secondary thorianite and possibly Ca and S for the formation of $CaSO_4$. The presence of nanoclusters of $CaSO_4$ has been earlier reported in S-rich monazite from ultra-high temperature granulite (Laurent et al., 2016). The SO_3 content in monazite in the SUD1 sample is below EPMA detection limit (i.e., <102 ppm), which suggests rather external source of S supplied by the fluid. However, it cannot be excluded that undetected with EPMA, small amounts of SO_3 in monazite were supplied in formation of $CaSO_4$ nanoinclusions. Only nanoinclusions of fluorapatite are not clearly related to any crack or closed grain boundaries (Fig. 3c, e–g, j), indicating that monazite was the source of Ca and P. The important role of nanoinclusions has been recently reported from monazite in ultra-high temperature granulite from Norway. The Ca-S-rich nanoclusters, 5–10 nm in size, homogeneously distributed in monazite have been recognized as a sink for radiogenic Pb released from monazite via Pb diffusion in the system closed at the microscale (Seydoux-Guillaume et al., 2019). In monazite in the migmatitic gneiss, $CaSO_4$ nanoinclusions can play such a role. Another sink for unsupported Pb that may interfere with U-Th-Pb characteristics of monazite are nanocrystals of fluorapatite or titanite, which can also accumulate Pb, and thorianite with radiogenic ^{208}Pb. This should be considered when evaluating the isotopic data.

Monazite in granulites, in contrast to the migmatitic gneiss sample, is homogeneous with no submicron inclusions in eight studied TEM foils (Fig. 6). The only evidence of fluid-induced processes resulting in compositional alterations in a submicron scale, which may affect U-Th-Pb isotope characteristics, is a single ca. 120 nm-thick crack filled with monazite (Fig. 6e–g). Such features are surprisingly positive for the use of investigated monazites from granulites in geochronology. Submicron characteristics of monazite from HP-HT metamorphic rocks were investigated only in a few studies and are still poorly recognized. The analytical volume of conventional in-situ techniques provided discordant U-Th-Pb data compromised by the presence of galena, but also affected by Pb-loss in monazite from an ultra-high temperature Archean granulite containing homogeneously distributed large number of Pb-bearing inclusions (Turuani et al., 2022). Recent experimental study also revealed extensive fluid-induced alterations of monazite at 750 °C resulting in high density of cheralite ($CaTh(PO_4)_2$) and fluid nanoinclusions, which remain unnoticed by common electron microscopy BSE imaging (Budzyń et al., 2021b). Here, monazite in the studied foils shows no such features. At some point this can be disappointing considering the lack of a simple explanation of the mechanisms responsible for the age disturbance in monazite Mnz2 in granulite GS290B or in the cores of monazites Mnz1 and Mnz2 in granulite SUD43 (Fig. 1d–f). The implication could be that common Pb is incorporated in the lattice of monazite. Possibly, the analytical volume sampled by the laser ablation includes discontinuities and more micro-fractures than the single micro-crack in foil F7 (Fig. 6e–g), that can contain common Pb.

4.2. Pb/U vs. Pb/Th monazite ages

A relatively small amount of nanometer-sized inclusions and compositional alterations of monazite limited to grain boundaries and the formation of nanometer-sized lamellae suggest that fluid-induced alteration may have had very limited influence on the monazite age record in the migmatitic gneiss SUD1. This is partially reflected in U-Th-Pb data, which are mostly <2% discordant (15 analyses), whereas 4 dates are with 2.2–5.9% disc. and there is only one highly discordant date with 13.6% disc. (Fig. 1a, b). All individual $^{207}Pb/^{235}$dates (except two discordant dates), $^{206}Pb/^{238}U$ and $^{208}Pb/^{232}Th$ dates stay within 2σ uncertainty range of their means (Fig. 8a–c). Monazite can be affected by excess of ^{206}Pb resulting in reverse discordance (Schoene, 2014), therefore, theoretically the $^{207}Pb/^{235}U$ age is expected to be younger and considered as more reliable than the $^{206}Pb/^{238}U$ age. The monazite SUD1, however, shows no evidence of such relation in Pb/U dates, except $^{207}Pb/^{235}U$ dates with highest discordance (Fig. 7a, b). They are probably affected by a moderate degree of radiation damage and/or incorporation of common Pb. The $^{208}Pb/^{232}Th$ mean dates 382.2 ± 9.1 Ma (all data) and 383 ± 11 Ma (<2% disc.) are roughly the same and only marginally older with respect to Pb/U means (Fig. 8a–f). The marginal difference can be related to a number of factors, including the choice of standard, heterogeneity of standard, uncertainty in calibration of standards or details of LA-ICPMS analytical conditions. The monazite TS-Mnz used as primary standard for calibration was characterized with ID-TIMS for the U—Pb system, but was not measured for Th—Pb system (Budzyń et al., 2021a). It has been shown that LA-ICPMS $^{207}Pb/^{235}U$ mean dates (three sessions: 899.8 ± 6.6 Ma, $n = 28$; 896.3 ± 6.5 Ma, $n = 22$; 901.9 ± 2.0, $n = 360$) are systematically slightly younger than ID-TIMS $^{207}Pb/^{235}U$ age 910.42 ± 0.34 Ma (2σ) of TS-Mnz, whereas LA-ICPMS $^{208}Pb/^{232}Th$ mean dates are more accurate (909.2 ± 5.8 Ma, n = 28; 915.1 ± 11 Ma, $n = 21$; 909.9 ± 1.5 Ma, $n = 366$; Budzyń et al., 2021a). Nevertheless, lower precision of LA-ICPMS compared to ID-TIMS hides discrepancies between both techniques and also the

reverse discordance. The isotope data of the reference material TS-Mnz partially explain the marginal discrepancy between Pb/U and Pb/Th dates in monazite from the migmatitic gneiss SUD1 (Fig. 8d–f), possibly as an instrumental feature of the LA-ICPMS technique measurements of monazite. Also, because the ^{208}Pb isotope has higher abundance in monazite than lighter isotopes ^{207}Pb and ^{206}Pb, the marginally older ^{208}Pb/^{232}Th mean more likely reflects the age of monazite crystallization. It cannot be excluded that some unsupported ^{208}Pb trapped in thorianite nanoinclusions may interfere with Pb/Th systematics of monazite. However, the size and low abundance of thorianite inclusions (Figs. 3g, 4d) suggest their negligible importance in the studied case. All these lead to the conclusion that ^{208}Pb/^{232}Th means, which are approximately the same for all and < 2% disc. data (382.2 ± 9.1 Ma and 383 ± 11 Ma, respectively; Fig. 8c, f), reflect a true age of metamorphic monazite in the migmatitic gneiss, which is in good agreement with previous geochronological constraints on the age of metamorphism in the Góry Sowie Block. The important conclusion is that partial alterations of monazite resulting in allanite overgrowths, submicron compositional alterations and formation of nanoinclusions do not affect U-Th-Pb age record.

Monazite in both granulites shows no submicron scale evidence of potential alterations (except one micro-crack filled with monazite), therefore we focus on the significance of the U-Th-Pb data with respect to earlier P-T constraints on the metamorphic records in granulites from the Góry Sowie Block. A pressure peak was determined in the range of 15 kbar/795 °C to 18–20 kbar/900–1000 °C (Kryza et al., 1996; O'Brien et al., 1997) at ca. 400–395 Ma (O'Brien et al., 1997; Gordon et al., 2005; Kryza and Fanning, 2007; Tabaud et al., 2020) followed by decompression to 6.5–8.5 kbar/775–910 °C (O'Brien et al., 1997). Recent thermodynamic modeling constrained decompression from conditions of ca. 17 kbar/840 °C to 11–12 kbar/850–860 °C (Jastrzębski et al., 2021). The investigation of granulite GS290B focused on the comparison of two monazite grains with concordant and discordant dates. The age distribution across both grains is uniform in each Mnz1 and Mnz2 (Fig. 1c, d), which yielded similar or nearly the same ^{206}Pb/^{238}U and ^{208}Pb/^{232}Th means pulled for their corresponding all data and < 2% disc. data. The high discordance in Mnz2 reflects incorporation of common Pb, which affected mostly the sensitive ^{207}Pb/^{235}U ratio (Fig. 7c, d), and possibly accumulated in the monazite lattice along the microcracks (Fig. 6e–g). The relation between Pb/U and marginally older Pb/Th concordant ages is similar to that discussed above in migmatitic gneiss. The ^{208}Pb/^{232}Th mean date 383.5 ± 8.8 Ma pulled for all data probably reflects age of monazite crystallization (Fig. 8i). The ^{207}Pb/^{235}U and ^{206}Pb/^{238}U means 370.6 ± 9.0 Ma and 370 ± 11 Ma (<2% disc.), respectively (Fig. 8j, k), are the same as the lower intercept age 371.0 ± 5.5 Ma and also consistent with earlier 370.0 ± 5.1 Ma age constraint on the decompression stage at high temperatures (Jastrzębski et al., 2021). It cannot be excluded that this suggests some ancient Pb-loss due to volume diffusion during prolonged ultra-high temperature metamorphic event in the granulite, despite that volume diffusion of Pb in monazite is very slow (Cherniak et al., 2004; Gardés et al., 2006). On the other hand, the relation between Pb/U and marginally older Pb/Th concordant ages is similar to that discussed above in migmatitic gneiss, and to LA-ICPMS characteristics of monazite standard TS-Mnz with consistently younger Pb/U dates compared to ID-TIMS Pb/U age (Budzyń et al., 2021a). In such case, Pb/U dates and U—Pb concordia ages can be actually misleading and we recommend using Pb/Th data in LA-ICPMS monazite dating.

The largest U-Th-Pb dataset was collected in granulite SUD43 and provides consistent and uniform mean dates, equal within their respective errors (Fig. 10). The exceptions are older ^{207}Pb/^{235}U mean date of 399.4 ± 3.7 Ma and younger ^{206}Pb/^{238}U mean date of 385.9 ± 4.1 Ma for all data from the cores, which is related to various degrees of high discordance in large number data. The latter is related to combination of partial Pb-loss, expressed as marginally younger ^{206}Pb/^{238}U dates, and addition of common Pb, which is effective mostly in ^{207}Pb/^{235}U ratio (Fig. 7e, f). The interesting is the difference in the U-Th-Pb records between Mnz1 and Mnz2 (previously studied in Jastrzębski et al., 2021), and other five grains studied. Monazite Mnz3–Mnz7 yielded U—Pb dates <5% disc. with only one 5.2% disc. date (Fig. 1g–k). We pushed the limits to consider <2% disc. analyses as concordant data, however, all ^{207}Pb/^{235}U dates (including those with 2–5.2% disc.) are within 2σ error. The isotopic data for the Mnz3–Mnz7 grains do not deserve further criticism.

There is no simple explanation of the mechanism(s) that induced high discordance of ^{207}Pb/^{235}U dates in the cores of monazites Mnz1 and Mnz2. Both grains are homogeneous in foils F8–F12 with no differences between cores and rims (Fig. 6h–l). The only difference is compositional:

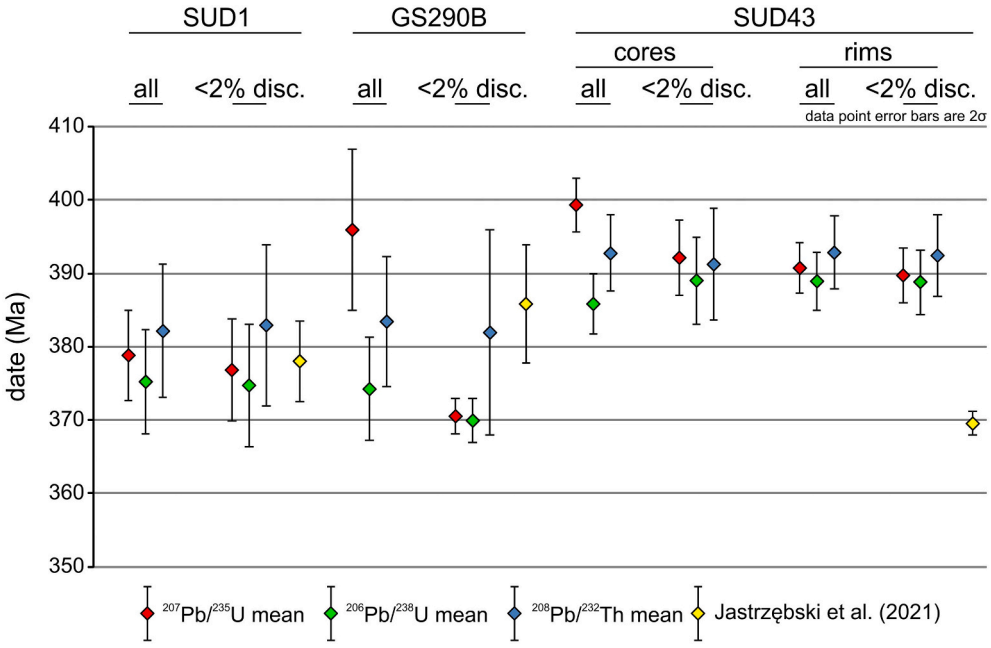

Fig. 10. Summary of the LA-ICPMS isotopic data from this study compared with results obtained for these samples, but higher monazite population with lesser number of analyses per grain in an earlier study of Jastrzębski et al. (2021).

dark (in high-contrast EPMA-BSE imaging) cores contain lower Th and higher U concentrations compared to bright rims (4.39–5.72 wt% ThO_2 and 0.98–0.88 wt% UO_2 vs. 9.21–10.08 wt% ThO_2 and 0.18–0.20 wt% UO_2). This is partially reflected in FWHM values of $\nu_1(PO_4)$ symmetric stretching Raman band 10.76–12.99 cm^{-1} and 15.34–16.46 cm^{-1}, that indicate lower efficiency of moderate degree of radiation damage in the cores than the rims, respectively. Nevertheless, neither Raman, EPMA nor TEM data provide evidence of processes, such as fluid-mediated alterations that may result in compositional alterations, which could explain the 6.8–12.4% disc. of U—Pb data in the cores. This suggests incorporation of common Pb in the lattice of monazite resulting in the discordance with shifting $^{207}Pb/^{235}U$ dates towards older ages, possibly combined with loss of radiogenic Pb, slightly shifting $^{206}Pb/^{238}U$ dates towards younger ages (Fig. 7e–f). Concerning all these, we recommend using a 5% or, if data allow, 2% discordance criterion to distinguish between the most concordant and other data to avoid misinterpretations using U—Pb dates with higher discordance.

One of the aspects of the U-Th-Pb data that also requires a short comment is a potential surface contamination by common Pb. This is particularly problematic in sample preparation for SIMS trace analysis of Pb (Schmitt and Vazquez, 2017). The common Pb contamination cannot be avoided in rock thin sections, but is less problematic in grain mounts with separated crystals. Laser ablation is sampling deeper into the crystals and the surface contamination is much less problematic. In this study, common Pb correction was not applied due to interference with ^{204}Hg in the carrier gas. Nevertheless, the uncorrected $^{206}Pb/^{204}Pb$ data demonstrate that ^{204}Pb content in monazite separated from granulite SUD43 (grain mount) is generally at the order of magnitude higher than in monazite in thin sections of migmatitic gneiss SUD1 and granulite GS290B (Fig. 11). These differences are rather related to individual characteristics of monazite in each sample and neither confirm nor deny a higher content of common Pb in monazite from the granulite SUD43. However, the results suggest negligible or no contamination from the surface in the thin sections during LA-ICPMS analysis.

Previous monazite dating of the granulite SUD43 reported highly discordant U—Pb ages due to incorporation of common Pb and late recrystallization at high temperature conditions. The intercept and concordia ages 369.6 ± 1.6 Ma and 370.0 ± 5.1 Ma, respectively, were interpreted as the age of decompression at high temperatures (Jastrzębski et al., 2021). In this work, $^{208}Pb/^{232}Th$ mean dates pulled for all data are 392.8 ± 5.2 Ma and 392.9 ± 5.0 Ma from cores and rims, respectively, and are considered to be the age of monazite crystallization during progressive metamorphism at the pressure peak. The $^{208}Pb/^{232}Th$ means are in good agreement with $^{207}Pb/^{235}U$ and $^{206}Pb/^{238}U$ mean ages, which are only marginally younger (Figs. 9, 10). The high discrepancy between ca. 390 Ma (this study) and ca. 370 Ma (Jastrzębski et al., 2021) monazite ages can be related to the choice of primary reference material or analytical conditions during LA-ICPMS sessions separated by several years difference, however, we found no evidence of such. The new ca. 393 Ma $^{208}Pb/^{232}Th$ age is in good agreement with earlier constraints on the HP-HT granulite facies metamorphism at ca. 400–395 Ma (O'Brien et al., 1997; Gordon et al., 2005; Kryza and Fanning, 2007; Tabaud et al., 2020).

Another aspect of this study is the importance of partially open grain boundaries at a nanometer scale that might have been pathways for fluids (Kruhl et al., 2013; Wirth et al., 2022). Compositional alterations of monazite that result in age discordance are most commonly considered to be recognizable in BSE imaging as altered rims or patchy domains (Budzyń et al., 2011, 2015, 2021b; Harlov et al., 2011; Williams et al., 2011; Grand'Homme et al., 2016, 2018). Here, monazite is little or not affected by fluid-induced alterations probably due to rapid cooling. Nevertheless, TEM investigations demonstrated that alteration of monazite is very well possible along partially open grain boundaries, either between monazite and another phase or along twins or cracks in monazite, which can be used for fluid migration. The presence of nanoinclusions of fluorapatite and calcite in monazite confirms the importance of the F and CO_2 component in the fluid during monazite alteration. Excess of ^{208}Pb resulting from the presence of thorianite nanoinclusions may affect $^{208}Pb/^{232}Th$ monazite age record, and it requires attention in evaluation of the material for geochronological analyses. In this work, the low abundance of thorianite nanoinclusions and the small size of submicron layers of altered monazite (via coupled dissolution-reprecipitation) compared to the ablated volume suggest that they cannot effectively affect the Pb/U and Pb/Th dates. However, special care should be taken as the intensity of the alterations with respect to the grain volume and mineral-fluid reaction rates can be

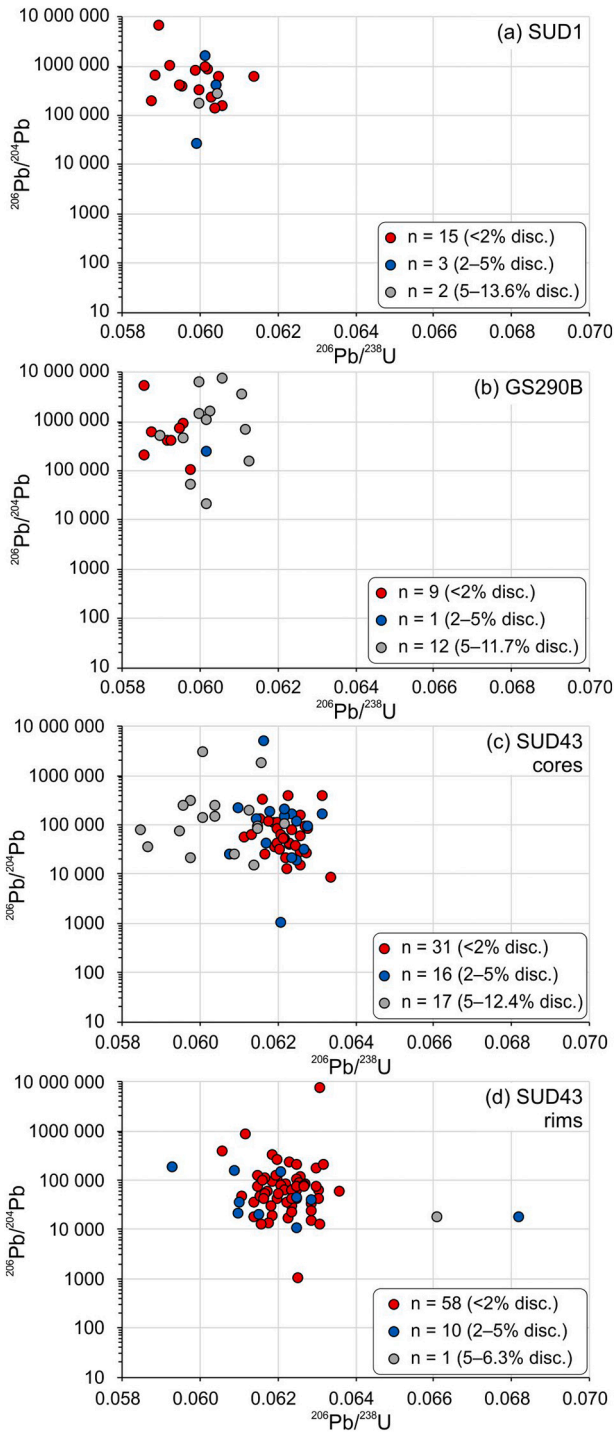

Fig. 11. Diagrams presenting $^{206}Pb/^{238}U$ vs. $^{206}Pb/^{204}Pb$ isotope ratios for monazite from migmatitic gneiss SUD1 and granulites GS290B and SUD43. Logarithmic y-axis is used.

higher, and may remain unnoticed in the microscale observations.

5. Conclusions

A compilation of TEM, EPMA, Raman microspectroscopy and extensive LA-ICPMS U-Th-Pb measurements provided important data, which allow us to better understand the submicron-scale processes that can affect the monazite U-Th-Pb geochronometer of high-grade metamorphic rocks. Altered monazite with allanite overgrowths in migmatitic gneiss that experienced temperature conditions of ca. 680–700 °C contains nanoinclusions of fluorapatite, thorianite, titanite, chlorite, goethite and $CaSO_4$, which are dispersed or located close to partially open or closed grain boundaries. These phases can be a source of unsupported Pb in monazite LA-ICPMS measurements, however, in case of the investigated sample, the submicron size, low abundance and high dispersion of these nanoinclusions question their influence on the U-Th-Pb characteristics of monazite. Fluid-induced alterations via coupled dissolution-reprecipitation occurred on the submicron-scale and resulted in compositional alteration of monazite. The limited textural effects of these alterations, which occurred during retrogressive metamorphic stage, are related to rapid cooling and had very limited or no effect on the monazite age record. The important insight of this study is that monazite from granulites is homogeneous in TEM foils with no solid or fluid nanoinclusions that may indicate fluid-induced alterations.

The presented study scrutinizing few carefully selected monazite grains demonstrates the importance of careful evaluation of the U-Th-Pb data with respect to various processes potentially affecting the age record, which can remain unnoticed as alterations in standard BSE imaging. The age disturbance related to addition of common Pb compromises particularly $^{207}Pb/^{235}U$ dates of monazite, shifting them towards older ages. The concordant $^{207}Pb/^{235}U$ and $^{206}Pb/^{238}U$ mean ages (limited to <2% or < 5% disc.) seem to be marginally younger than expected true age of monazite crystallization, which can be explained by some Pb-loss or LA-ICPMS analytical conditions (choice of the standard, analytical conditions in each session, etc.). Because of higher Th content in monazite, the $^{208}Pb/^{232}Th$ ratio is less sensitive to the incorporation of initial Pb. The new $^{208}Pb/^{232}Th$ mean ages are consistent with earlier geochronology, and are considered as reflecting the true ages in all studied samples. This study demonstrates that LA-ICPMS $^{208}Pb/^{232}Th$ dates can be the most effective in monazite geochronology and the application of TEM is required for better understanding the age data and to exclude potential influence of submicron inclusions of Pb-bearing phases.

Declaration of Competing Interest

The authors declare that they have no known competing financial interests or personal relationships that could have appeared to influence the work reported in this paper.

Acknowledgements

M. Jastrzębski and A. Żelaźniewicz are acknowledged for providing samples of gneiss and granulites for this study. We acknowledge B. Kamber for editorial handling, and B. Bingen and anonymous reviewer for their constructive comments. This study was financially supported by the Polish National Science Centre (NCN) research grant no. 2017/27/B/ST10/00813 (to B.B.). J.S. was supported by the CAS support RVO 67985831.

Appendix A. Supplementary data

Supplementary data to this article can be found online at https://doi.org/10.1016/j.chemgeo.2022.121015.

References

Barnes, C.J., Majka, J., Jeanneret, P., Ziemniak, G., Kooijman, E., Kośmińska, K., Kielman-Schmitt, M., Schneider, D.A., 2021. Using Th-U-Pb geochronology to extract crystallization ages of Paleozoic metamorphic monazite contaminated by initial Pb. Chem. Geol. 582, 120450.

Bröcker, M., Żelaźniewicz, A., Enders, M., 1998. Rb-Sr and U-Pb geochronology of migmatitic gneisses from the Góry Sowie (West Sudetes, Poland): the importance of Mid-Late Devonian metamorphism. J. Geol. Soc. Lond. 155, 1025–1036.

Broska, I., Siman, P., 1998. The breakdown of monazite in the West-Carpathian Veporic orthogneisses and Tatric granites. Geol. Carpath. 49, 161–167.

Budzyń, B., Hetherington, C.J., Williams, M.L., Jercinovic, M.J., Michalik, M., 2010. Fluid-mineral interactions and constraints on monazite alteration during metamorphism. Mineral. Mag. 74, 659–681.

Budzyń, B., Harlov, D.E., Williams, M.L., Jercinovic, M.J., 2011. Experimental determination of stability relations between monazite, fluorapatite, allanite, and REE-epidote as a function of pressure, temperature, and fluid composition. Am. Mineral. 96, 1547–1567.

Budzyń, B., Konečný, P., Kozub-Budzyń, G., 2015. Stability of monazite and disturbance of the Th-U-Pb system under experimental conditions of 250–350 °C and 200–400 MPa. Ann. Soc. Geol. Pol. 85, 405–424.

Budzyń, B., Harlov, D.E., Kozub-Budzyń, G., Majka, J., 2017. Experimental constraints on the relative stabilities of the two systems monazite-(Ce) – allanite-(Ce) – fluorapatite and xenotime-(Y) – (Y,HREE)-rich epidote – (Y,HREE)-rich fluorapatite, in high Ca and Na-Ca environments under P-T conditions of 200–1000 MPa and 450–700 °C. Mineral. Petrol. 111, 183–217.

Budzyń, B., Sláma, J., Kozub-Budzyń, G.A., Konečný, P., Holický, I., Rzepa, G., Jastrzębski, M., 2018. Constraints on the timing of multiple thermal events and re-equilibration recorded by high-U zircon and xenotime: case study of pegmatite from Piława Górna (Góry Sowie Block, SW Poland). Lithos 310–311, 65–85.

Budzyń, B., Sláma, J., Corfu, F., Crowley, J., Schmitz, M., Williams, M.L., Jercinovic, M. J., Kozub-Budzyń, G.A., Konečny, P., Rzepa, G., Włodek, A., 2021a. TS-Mnz – a new monazite age reference material for U-Th-Pb microanalysis. Chem. Geol. 572, 120195.

Budzyń, B., Wirth, R., Sláma, J., Birski, Ł., Tramm, F., Kozub-Budzyń, G.A., Rzepa, G., Schreiber, A., 2021b. LA-ICPMS, TEM and Raman study of radiation damage, fluid-induced alteration and disturbance of U-Pb and Th-Pb ages in experimentally metasomatised monazite. Chem. Geol. 583, 120464.

Cherniak, K., Watson, E., Grove, M., Harrison, M.T., 2004. Pb diffusion in monazite: a progress report on a combined RBS/SIMS study. Geochim. Cosmochim. Acta 68, 829–840.

Didier, A., Bosse, V., Boulvais, P., Bouloton, J., Paquette, J.-L., Montel, J.-M., Devidal, J.-L., 2013. Disturbance versus preservation of U–Th–Pb ages in monazite during fluid–rock interaction: textural, chemical and isotopic in situ study in microgranites (Velay Dome, France). Contrib. Mineral. Petrol. 165, 1051–1072.

Finger, F., Broska, I., Roberts, M.P., Schermaier, A., 1998. Replacement of primary monazite by apatite-allanite-epidote coronas in an amphibolite facies granite gneiss from the eastern Alps. Am. Mineral. 83, 248–258.

Gardés, E., Jaoul, O., Montel, J.-M., Seydoux-Guillaume, A.-M., Wirth, R., 2006. Pb diffusion in monazite: An experimental study of $Pb^{2+} + Th^{4+} \Longleftrightarrow 2Nd^{3+}$ interdiffusion. Geochim. Cosmochim. Acta 70, 2325–2336.

Gonçalves, G.O., Lana, C., Scholz, R., Buick, I.S., Gerdes, A., Kamo, S.L., Corfu, F., Marinhof, M.M., Chaves, A.O., Valeriano, C., Nalini Jr., H.A., 2016. An assessment of monazite from the Itamb'e pegmatite district for use as U–Pb isotope reference material for microanalysis and implications for the origin of the "Moacyr" monazite. Chem. Geol. 424, 30–50.

Gonçalves, G.O., Lana, C., Scholz, R., Buick, I.S., Gerdes, A., Kamo, S.L., Corfu, F., Rubatto, D., Wiedenbeck, M., Nalini Jr., H.N., Oliveira, L.C.A., 2017. The Diamantina monazite: a new low-Th reference material for microanalysis. Geostand. Geoanal. Res. 42, 25–47.

Gordon, S.M., Schneider, D.A., Manecki, M., Holm, D.K., 2005. Exhumation and metamorphism of an ultrahigh-grade terrane: geochronometric investigations of the Sudete Mountains (Bohemia), Poland and Czech Republic. J. Geol. Soc. 162, 841–855.

Grand'Homme, A., Janots, E., Seydoux-Guillaume, A.-M., Guillaume, D., Bosse, V., Magnin, V., 2016. Partial resetting of the U-Th-Pb systems in experimentally altered monazite: Nanoscale evidence of incomplete replacement. Geology 44, 431–434.

Grand'Homme, A., Janots, E., Seydoux-Guillaume, A.M., Guillaume, D., Magnin, V., Hövelmann, J., Höschen, C., Boiron, M.C., 2018. Mass transport and fractionation during monazite alteration by anisotropic replacement. Chem. Geol. 484, 51–68.

Harlov, D.E., Wirth, R., Hetherington, C.J., 2011. Fluid-mediated partial alteration in monazite: the role of coupled dissolution-reprecipitation in element redistribution and mass transfer. Contrib. Mineral. Petrol. 162, 329–348.

Janots, E., Brunet, F., Goffé, B., Poinssot, C., Burchard, M., Cemic, L., 2007. Thermochemistry of monazite-(La) and dissakisite-(La): implications for monazite and allanite stability in metapelites. Contrib. Mineral. Petrol. 154, 1–14.

Janots, E., Engi, M., Berger, A., Allaz, J., Schwarz, J.O., Spandler, C., 2008. Prograde metamorphic sequence of REE minerals in pelitic rocks of the Central Alps: implications for allanite–monazite–xenotime phase relations from 250 to 610°C. J. Metamorph. Geol. 26, 509–526.

Jastrzębski, J., Żelaźniewicz, A., Budzyń, B., Sláma, J., Konečny, P., 2020. Age constraints on the Pre-Variscan and Variscan thermal events in the Kamieniec Ząbkowicki Metamorphic belt (the Fore-Sudetic Block, SW Poland). Ann. Soc. Geol. Pol. 90, 27–49.

Jastrzębski, M., Budzyń, B., Żelaźniewicz, A., Konečný, P., Sláma, J., Kozub-Budzyń, G. A., Skrzypek, E., Jaźwa, A., 2021. Eo-Variscan metamorphism in the Bohemian

Massif: thermodynamic modeling and monazite geochronology of gneisses and granulites of the Góry Sowie Massif, SW Poland. J. Metamorph. Geol. 39, 751–779.
Kruhl, J.H., Wirth, R., Morales, L.F.G., 2013. Quartz grain boundaries as fluid pathways in metamorphic rocks. J. Geophys. Res. Solid Earth 118 (5), 1–11.
Kryza, R., 1981. Migmatization in gneisses of the northern part of the Sowie Góry, Sudetes. Geol. Sudet. 16, 7–91.
Kryza, R., Fanning, C.M., 2007. Devonian deep-crustal metamorphism and exhumation in the Variscan Orogen: evidence from SHRIMP zircon ages from the HT-HP granulites and migmatites of the Góry Sowie (Polish Sudetes). Geodin. Acta 20, 159–175.
Kryza, R., Pin, C., Vielzeuf, D., 1996. High-pressure granulites from the Sudetes (south-West Poland): evidence of crustal subduction and collision thickening in the Variscan Belt. J. Metamorph. Geol. 14, 531–546.
Kylander-Clark, A.R.C., 2017. Petrochronology by laser-ablation inductively coupled plasma mass spectrometry. In: Kohn, M.J., Engi, M., Lanari, P. (Eds.), Petrochronology: Methods and Applications, Reviews in Mineralogy and Geochemistry, vol. 83, pp. 183–198.
Laurent, A.T., Seydoux-Guillaume, A.-M., Duchene, S., Bingen, B., Bosse, V., Datas, L., 2016. Sulphate incorporation in monazite lattice and dating the cycle of sulphur in metamorphic belts. Contrib. Mineral. Petrol. 171, 94.
Ludwig, K.R., 2012. Isoplot 3.75. A Geochronological Toolkit for Microsoft Excel, 5. Berkeley Geochronological Center, pp. 1–75. Special Publication.
Marheine, D., Kachlik, V., Maluski, H., Patočka, F., Żelaźniewicz, A., 2002. The $^{40}Ar/^{39}Ar$ ages from the West Sudetes (NE Bohemian Massif): constraints on the Variscan polyphase tectonothermal development. In: Winchester, J.A., Pharaon, T.C., Verniers, J. (Eds.), Palaeozoic Amalganation of Central Europe, Geological Society of London, Special Publications, vol. 201, pp. 133–155.
Nasdala, L., Wenzel, M., Vavra, G., Irmer, G., Wenzel, T., Kober, B., 2001. Metamictisation of natural zircon: Accumulation versus thermal annealing of radioactivity-induced damage. Contrib. Mineral. Petrol. 141, 125–144.
Nasdala, L., Akhmadaliev, S., Burakov, B.E., Chanmuang, N., Škoda, R., 2020. The absence of metamictisation in natural monazite. Sci. Rep. 10, 14676.
O'Brien, P.J., Kröner, A., Jaeckel, P., Hegner, E., Żelaźniewicz, A., Kryza, R., 1997. Petrological and isotopic studies on Palaeozoic high-pressure granulites, Gory Sowie Mts, Polish Sudetes. J. Petrol. 38, 433–456.
Ruschel, K., Nasdala, L., Kronz, A., Hanchar, J.M., Többens, D.M., Škoda, R., Finger, F., Möller, A., Ruschel, K., Nasdala, L., Kronz, A., Hanchar, J.M., Többens, D.M., Škoda, R., Finger, F., Möller, A., 2012. A Raman spectroscopic study on the structural disorder of monazite-(Ce). Mineral. Petrol. 105, 41–55.
Schmitt, A.K., Vazquez, J.A., 2017. Secondary ionization mass spectrometry analysis in petrochronology. In: Kohn, M.J., Engi, M., Lanari, P. (Eds.), Petrochronology: Methods and Applications, Reviews in Mineralogy and Geochemistry, vol. 83, pp. 199–230.
Schneider, D.A., Zahniser, S.J., Glascock, J.M., Gordon, S.M., Manecki, M., 2006. Thermochronology of the west Sudetes (Bohemian Massif): rapid and repeated eduction in the eastern Variscides, Poland and Czech Republic. Am. J. Sci. 306, 846–873.
Schoene, B., 2014. U–Th–Pb geochronology. In: Holland, H.D., Turekian, K.K. (Eds.), Treatise on Geochemistry (Second Edition), vol. 4.10. Elsevier, pp. 341–378.
Seydoux-Guillaume, A.-M., Montel, J.-M., Bingen, B., Bosse, V., De Parseval, P., Paquette, J., Janots, E., Wirth, R., 2012. Low-temperature alteration of monazite: fluid mediated coupled dissolution–precipitation, irradiation damage, and disturbance of the U–Pb and Th–Pb chronometers. Chem. Geol. 330–331, 140–158.
Seydoux-Guillaume, A.-M., Bingen, B., Bosse, V., Janots, E., Laurent, A.T., 2018a. Transmission electron microscope imaging sharpens geochronological interpretation of zircon and monazite. In: Moser, D.E., Corfu, F., Darling, J.R., Reddy, S.M., Tait, K. (Eds.), Microstructural Geochronology: Planetary Records Down to Atom Scale, Geophysical Monograph 232, First edition. American Geophysical Union. John Wiley & Sons, Inc, pp. 261–275.
Seydoux-Guillaume, A.-M., Deschanelsls, X., Baumier, C., Neumeier, S., Weber, W.J., Peuget, S., 2018b. Why natural monazite never becomes amorphous: Experimental evidence for alpha self-healing. Am. Mineral. 103, 824–827.
Seydoux-Guillaume, A.-M., Fougerouse, D., Laurent, A.T., Gardés, E., Reddy, S.M., Saxey, D.W., 2019. Nanoscale resetting of the Th/Pb system in an isotopically-closed monazite grain: a combined atom probe and transmission electron microscopy study. Geosci. Front. 10, 65–76.
Skrzypek, E., Bosse, V., Tetsuo Kawakami, T., Martelat, J.E., Štípská, P., 2017. Transient allanite replacement and prograde to retrograde monazite (re)crystallization in medium-grade metasedimentary rocks from the Orlica-Śnieżnik Dome (Czech Republic/Poland): textural and geochronological arguments. Chem. Geol. 449, 41–57.
Spear, F.S., 2010. Monazite–allanite phase relations in metapelites. Chem. Geol. 279, 55–62.
Tabaud, A.S., Štípská, P., Mazur, S., Schulmann, K., Míková, J., Wong, J., Sun, M., 2020. Evolution of a Cambro-Ordovician active margin in northern Gondwana: Geochemical and zircon geochronological evidence from the Góry Sowie metasedimentary rocks, Poland. Gondwana Res. 90, 1–26.
Turuani, M.J., Laurent, A.T., Seydoux-Guillaume, A.-M., Fougerouse, D., Saxey, D., Reddy, S.M., Harley, S.L., Reynaud, S., Rickard, W.D.A., 2022. Partial retention of radiogenic Pb in galena nanocrystals explains discordance in monazite from Napier complex (Antarctica). Earth Planet. Sci. Lett. 588, 117567.
Williams, M.L., Jercinovic, M.J., Harlov, D.E., Budzyń, B., Hetherington, C.J., 2011. Resetting monazite ages during fluid-related alteration. Chem. Geol. 283, 218–225.
Williams, M.L., Jercinovic, M.J., Mahan, K.H., Dumond, G., 2017. Electron microprobe petrochronology. In: Kohn, M.J., Engi, M., Lanari, P. (Eds.), Petrochronology: Methods and Applications, Reviews in Mineralogy and Geochemistry, vol. 83, pp. 153–182.
Wirth, R., 2004. Focused Ion Beam (FIB): a novel technology for advanced application of micro- and nanoanalysis in geosciences and applied mineralogy. Eur. J. Mineral. 16, 863–876.
Wirth, R., 2009. Focused Ion Beam (FIB) combined with SEM and TEM: Advanced analytical tools for studies of chemical composition, microstructure and crystal structure in geomaterials on a nanometre scale. Chem. Geol. 261, 217–229.
Wirth, R., Kruhl, J.H., Morales, L.F.G., Schreiber, A., 2022. Partially open grain and phase boundaries as fluid pathways in metamorphic and magmatic rocks. J. Metamorph. Geol. 40, 67–85.
Żelaźniewicz, A., 1990. Deformation and metamorphism in the Góry Sowie gneiss complex, Sudetes, SW Poland. Neues Jahrbuch für Paläontologie – Abhandlungen 179, 129–157.